INTERACTIONS OF INTENSE COHERENT LIGHT WITH IODINE VAPOR, NEODYMIUM - DOPED GLASS, AND BENZENE

LORIN W. BROWN

INTERACTIONS OF INTENSE COHERENT LIGHT WITH IODINE VAPOR, NEODYMIUM-DOPED GLASS, AND BENZENE

by

Lorin W Brown

A dissertation submitted to the faculty of the
University of Utah in partial fulfillment of the requirements
for the degree of

Doctor of Philosophy

Department of Physics

University of Utah
June 1970

This Dissertation for the

Doctor of Philosophy Degree

by

Lorin W Brown

has been approved

March 1970

ACKNOWLEDGMENTS

The author would like to thank Professor Grant R. Fowles for his suggestions and guidance during the course of this research.

He is also grateful for the assistance of Dr. Bruce D. Hopkins, Dr. Robert Pixton, and Captain William E. Adams, USAF. Hans Morrow of the Chemistry Department also deserves thanks for his glass-blowing work.

The author is most grateful to his wife for her pleasant encouragement and considerable patience.

Gratitude is expressed to the Navy Department for the Naval Postgraduate Educational Program which provided the author the opportunity to do this research.

TABLE OF CONTENTS

LIST OF ILLUSTRATIONS

LIST OF TABLES

ABSTRACT

This dissertation reports the interaction of intense radiation with iodine vapor, neodymium-doped glass, and benzene. A new stimulated effect was observed in benzene. Broad-band stimulated emission in the region of 9100Å to 10,900Å was observed when the benzene was pumped with light at 6943Å from a ruby Q-switched laser. The emission consisted of a pulse of less than 10 nsec duration. Peak power of the pulse was approximately 500 KW when the ruby laser output was 40 MW. Threshold was estimated at 25 ± 10 MW/cm^2.

Stimulated emission at 1.06 microns was observed from neodymium-doped glass when it was pumped with Raman-shifted light at 7458Å, 8053Å, and 8751Å. The Raman-shifted light was obtained by passing light from a Q-switched ruby laser through benzene. The emission consisted of a pulse of less than 10 nsec duration.

Absorption of laser radiation at 6943Å and 5310Å was measured in iodine vapor but no stimulated effects were apparent.

I. INTRODUCTION

Shortly after the first laser was operated successfully by Maiman[1], Hellwarth[2] proposed controlling the cavity of the laser by Q-switching to produce a very intense pulse of light. The intensity of the light produced by Q-switching can be so great as to produce a large number of non-linear optical effects in matter.

The first of these effects as identified by Eckhardt and Hellwatch, et al,[3] was stimulated Raman emission in nitrobenzene, benzene, and several other organic liquids. Stimulated Brillouin scattering was first reported in quartz and sapphire by Chiao, Townes, and Stoicheff.[4] Stimulated Rayleigh scattering and Brillouin scattering in nitrobenzene were reported by Cho, Foltz, Rank, and Wiggins.[5] Self-focusing of intense light beams, as proposed by Askargan,[6] was found by Chiao, Townes, and Garmire[7] to be inextricably involved in the other non-linear processes. These effects have since been found in numerous other materials and the search continues.

In 1966, Sorokin and Lankard[8] obtained stimulated fluorescence in dyes by passing intense light from a Q-switched ruby laser through them. In 1969, Briquet, Jego, and Terneaud[9] observed the generation of ultra short pulses at 1.06 microns in neodymium-doped glass when it was pumped with light which had been frequency doubled from a

Q-switched neodymium laser.

This dissertation reports experimental observations on the interaction of intense radiation with iodine, benzene, and neodymium-doped glass. New stimulated effects were observed in the case of benzene and neodymium-doped glass. Absorption of the laser radiation was measured in iodine vapor, but no stimulated effects were apparent under the experimental conditions of this investigation.

II. RADIATION INTERACTIONS

A. Emission

A comprehensive study of radiation interactions with matter is obviously a topic too broad to discuss in detail here, and the variety of ways in which it can be treated are too numerous to treat in this paper. We will, therefore, give a brief treatment of the interaction of radiation with matter similar to that used by Dirac,[10] as modified by Marcuse.[11]

When considering more than a single isolated system, it is often convenient to write the Hamiltonian as

$$H = H_o + H_{int} \tag{1}$$

where H_o is the sum of the Hamiltonians of the individual systems, and H_{int} is the interaction Hamiltonian. The Schroedinger equation is then

$$i\hbar \frac{d}{dt} |\Psi\rangle = (H_o + H_{int}) |\Psi\rangle \tag{2}$$

We can transform this by a unitary transformation to the interaction representation where the state vector is now

$$|\Psi'(t)\rangle = e^{i\frac{H_o}{\hbar}t} |\Psi\rangle \tag{3}$$

and the interaction Hamiltonian is

$$H'_{int} = e^{i\frac{H_o}{\hbar}t} H_{int} e^{-i\frac{H_o}{\hbar}t} \tag{4}$$

In this representation, the Schroedinger equation is

$$i\hbar \frac{d}{dt} |\Psi'(t)\rangle = H'_{int} |\Psi'(t)\rangle \tag{5}$$

This can be integrated to give

$$|\Psi'(t)\rangle = |\Psi'(0)\rangle + \frac{1}{i\hbar}\int_o^t H'_{int}(\tau) |\Psi'(\tau)\rangle d\tau \tag{6}$$

It is not the intent of this paper to discuss the solutions of this equation. Suffice it to say that in practice the equation is solved approximately by an iteration technique. This involves replacing $|\Psi'(\tau)\rangle$ with $|\Psi'(0)\rangle$ and solving for $|\Psi'(t)\rangle$ for a first order approximation

$$|\Psi'(t)\rangle_1 = \left[1 + \frac{1}{i\hbar}\int_o^t H'_{int}(\tau)\, d\tau\right] |\Psi'(0)\rangle \tag{7}$$

For the second order approximation, we replace $|\Psi'(\tau)\rangle$ with $|\Psi'(t)\rangle_1$ and solve for $|\Psi'(t)\rangle_2$

$$|\Psi'(t)\rangle_2 = \left[1 + \frac{1}{i\hbar}\int_o^t H'_{int}(\tau)\, d\tau + \frac{1}{(i\hbar)^2}\int_o^t \int_o^{\tau_1} H'_{int}(\tau_1) H'_{int}(\tau_2)\, d\tau_1\, d\tau_2\right] |\Psi'(0)\rangle$$

This process can be repeated to as high an order as desired. It is then convenient to introduce the scattering operator

$$S = \left[1 + \frac{1}{i\hbar}\int_o^t H'_{int}(\tau)\, d\tau + \frac{1}{(i\hbar)^2}\int_o^t \int_o^{\tau_1} H'_{int}(\tau_1) H'_{int}(\tau_2)\, d\tau_1\, d\tau_2 + \ldots\right] \tag{9}$$

and to write

$$|\Psi'(t)\rangle = S\ |\Psi'(0)\rangle \tag{10}$$

For a problem of absorption, emission, or scattering, we are generally interested in the probability that a system which was initially known to be in state $|\Psi'(0)\rangle$ at t = 0 (normally an eigenstate of H_o) will be found in an eigenstate $|E_f\rangle$ at time t. $|E_f\rangle$ is an eigenvector of H_o corresponding to the energy eigenvalue, E_f. This probability is

$$P_f = |\langle E_f|\Psi'(t)\rangle|^2 \tag{11}$$

which, from (10), can be written

$$P_f = |\langle E_f|\ S\ |\Psi'(0)\rangle|^2 \tag{12}$$

According to our previous choice, $|\Psi'(0)\rangle = |E_i\rangle$ was an eigenstate of H_o also. Hence,

$$P_f = |\langle E_f|\ S\ |E_i\rangle|^2 \tag{13}$$

If we now take this to a first order approximation, we have

$$S = 1 + \frac{1}{i\hbar}\int_o^t H'_{int}\ (\tau)\ d\tau = 1 + \frac{1}{i\hbar}\int_o^t e^{i\frac{H_o}{\hbar}\tau}\ H_{int}\ e^{-i\frac{H_o}{\hbar}\tau}\ d\tau \tag{14}$$

and

$$P_f = \left|\langle E_f|E_i\rangle + \frac{1}{i\hbar}\int_o^t \langle E_f|e^{i\frac{H_o}{\hbar}\tau}\ H_{int}\ e^{-i\frac{H_o}{\hbar}\tau}|\ E_i\rangle\ d\tau\right|^2 \tag{15}$$

We know, however, that two different eigenvectors are orthogonal, that is, in our case, $\langle E_f | E_i \rangle = 0$. We also know that when

$$H_o | E_n \rangle = E_n | E_n \rangle \tag{16}$$

then

$$f(H_o) | E_n \rangle = f(E_n) | E_n \rangle \tag{17}$$

Hence

$$P_f = \left| \frac{1}{i\hbar} \langle E_f | H_{int} | E_i \rangle \int_o^t e^{i(E_f - E_i)\frac{\tau}{\hbar}} d\tau \right|^2 \tag{18}$$

and by integration

$$P_f = \left| \frac{1}{i\hbar} \langle E_f | H_{int} | E_i \rangle \frac{\hbar \left[e^{i(E_f - E_i)\frac{\tau}{\hbar}} - 1 \right]}{i(E_f - E_i)} \right|^2 \tag{19}$$

By means of trigonometric identities, this can be put in to the familiar form

$$P_f = 4 \left| \langle E_f | H_{int} | E_i \rangle \right|^2 \left[\frac{\sin(E_f - E_i) \frac{t}{2\hbar}}{(E_f - E_i)} \right]^2 \tag{20}$$

At this point, it is convenient to introduce the Dirac delta function in the normalized form

$$\delta(E_f - E_i) = \lim_{\frac{t}{2\hbar} \to \infty} \frac{1}{\pi} \frac{\sin(E_f - E_i)\frac{t}{2\hbar}}{E_f - E_i} \tag{21}$$

We will be concerned not only with the actual limiting case, $t \to \infty$, but for all cases of sufficiently large t. For these cases, the use of the delta function is a good enough approximation for our purposes.

The probability is then

$$P_f = 4\pi \left| \langle E_f | H_{int} | E_i \rangle \right|^2 \frac{\sin(E_f - E_i)\frac{t}{2\hbar}}{(E_i - E_f)} \delta(E_f - E_i) \tag{22}$$

which by use of the properties of the delta function becomes

$$P_f = \frac{2\pi t}{\hbar} \left| \langle E_f | H_{int} | E_i \rangle \right|^2 \quad \delta(E_f - E_i) \tag{23}$$

This is the transition probability from $|E_i\rangle$ to $|E_f\rangle$, but if we are concerned with the total probability of a transition we must sum over all possible transitions.

$$P = \Sigma P_f \tag{24}$$

This total probability is normally arrived at by assuming the density of final states is great enough to introduce the number of states $\rho_f \, dE_f$ in the interval dE_f, and by replacing the sum with an integral. Hence

$$P = \int P_f \rho_f dE_f \tag{25}$$

and

$$P = \int_{-\infty}^{\infty} \frac{2\pi t}{\hbar} \left| \langle E_f | H_{int} | E_i \rangle \right|^2 \quad \delta(E_f - E_i) \rho_f dE_f \tag{26}$$

which gives

$$P = \frac{2\pi t}{\hbar} \left| \langle E_f | H_{int} | E_i \rangle \right|^2 \rho_f \tag{27}$$

If we are interested in the transition probability per unit time, this becomes

$$w = \frac{dP}{dt} = \frac{2\pi}{\hbar} |\langle E_f| H_{int} |E_i\rangle|^2 \rho_f \tag{28}$$

In the case of an electromagnetic wave interacting with a bound electron, the interaction Hamiltonian is given by

$$H_{int} = -\frac{e}{m}(\vec{p} \cdot \vec{A}) + \frac{e^2}{2m} \vec{A}^2 \tag{29}$$

where $\vec{p}$ is the momentum of the electron and $\vec{A}$ is the vector potential of the field. The term $\frac{e^2}{2m} \vec{A}^2$ is negligible in all cases which we will consider, except Rayleigh scattering.

It is convenient to take the plane wave representation of $\vec{A}$ expressed in terms of creation and annihilation operators, namely

$$\vec{A} = \sum_{s=1}^{2} \sum_{m} \sqrt{\frac{\hbar}{2\varepsilon\omega_m V}}\, \vec{e}_{ms} \left(a^{+}_{ms} e^{-i\vec{k}_m \cdot \vec{r}} + a_{ms} e^{i\vec{k}_m \cdot \vec{r}}\right) \tag{30}$$

and to express the initial and final states of the system as products of the electron state and photon state:

$$|E_i\rangle = |\Psi_i\rangle |\, n_1, n_2, \ldots n_{\nu\sigma} \ldots \rangle \tag{31}$$

$$|E_f\rangle = |\Psi_f\rangle |\, n_1, n_2, \ldots n_{\nu\sigma+1}, \ldots \rangle \tag{32}$$

where the n_i are photon occupation numbers of all the radiation modes. We can now obtain the transition probability per unit time for emission by direct substitution into equation (28). The result is

$$w = \frac{\pi e^2}{m^2 \varepsilon \omega_\nu V} (n_{\nu\sigma} + 1)\rho_f \; | \langle \Psi_f | \vec{e}_{\nu\sigma} \cdot \vec{p} e^{-i\vec{k}_\nu \cdot \vec{r}} |\Psi_i\rangle|^2 \tag{33}$$

This can be written in an integral form as

$$w = \frac{\pi e^2 \hbar^2}{m^2 \varepsilon \omega_\nu V} (n_{\nu\sigma} + 1)\rho_f \left| \int \Psi_f^* (\vec{e}_{\nu\sigma} \cdot \nabla \Psi_i)\, e^{-i\vec{k}_\nu \cdot \vec{r}}\, dV \right|^2 \tag{34}$$

The density of states is obtained by considering emission into a solid angle $d\Omega$ around $\vec{k}_\nu$. The final electron level is considered well defined, so the density will be determined by the density of photon states available. This is given by

$$\rho_f = \frac{2V}{(2\pi)^3} \left(\frac{\varepsilon}{\varepsilon_o}\right)^{\frac{3}{2}} \frac{\omega_\nu^2}{\hbar c^3}\, d\Omega \tag{35}$$

If we now restrict ourselves to spontaneous emission ($n_{\nu\sigma} = 0$) and to dipole radiation $e^{i\vec{k}\cdot\vec{r}} \approx 1$, we obtain

$$w_{spe} = \frac{e^2 \hbar \omega_\nu}{4\pi^2 \varepsilon_o m^2 c^3} \sqrt{\frac{\varepsilon}{\varepsilon_o}} \left| \int \Psi_f^*\, e_{\nu\sigma} \cdot \nabla \Psi_i dV \right|^2 d\Omega \tag{36}$$

For the dipole case only, this is equivalent to the more familiar form

$$w_{spe} = \frac{\omega_\nu^3 \sqrt{\frac{\varepsilon}{\varepsilon_o}}}{4\pi^2 \varepsilon_o \hbar c^3} \left| \mu_{fi}^{\nu\sigma} \right|^2 d\Omega \tag{37}$$

where the dipole matrix element

$$\mu_{fi}^{\nu\sigma} = e \int \Psi_f^* (\vec{e}_{\nu\sigma} \cdot \vec{r}) \Psi_i\, dV \tag{38}$$

was obtained by starting with an approximate interaction Hamiltonian of the form

$$H_{int} = - e\vec{E} \cdot \vec{r} \tag{39}$$

where

$$\vec{E} = - \frac{\partial_\nu \vec{A}}{\partial t} \tag{40}$$

If we integrate over all possible orientations of the emitted radiation, and take into account the possibility of degenerate states, we end up with the total probability for spontaneous emission at frequency ω_ν:

$$\langle w_{spe} \rangle = \frac{\omega_\nu^3 g_1 \sqrt{\frac{\varepsilon}{\varepsilon_o}}}{4\pi^2 \varepsilon_o \hbar c^3} \left| \mu_{fi}^{\nu\sigma} \right|^2 d\Omega \tag{41}$$

The dipole matrix element, $\mu_{fi}^{\nu\sigma}$, is still a function of the orientation of the atoms. In a gas, the orientation is random; so an average is usually performed over all possible orientations. This requires the use of an average dipole matrix $|\bar{\mu}_{fi}|$ which is independent of the solid angle. If we introduce the average radiation life time τ_{spe} and integrate over the solid angle, we then obtain

$$\frac{1}{\tau_{spe}} = \langle w_{spe} \rangle = \frac{\omega_\nu^3 \, g_1 \sqrt{\frac{\varepsilon}{\varepsilon_o}}}{\pi \varepsilon_o \hbar c^3} \left| \bar{\mu}_{fi} \right|^2 \tag{42}$$

B. Absorption

It is obvious that absorption cannot be a spontaneous process. There must always be an occupied mode in the initial state before absorption is allowed. The derivation of the expression for

he transition probability for absorption closely parallels that for spontaneous emission, except that the density of initial states enters into the equation instead of the density of final states. They are of the same form, except that for absorption there is a factor of $n_{\nu\sigma}$ in place of $n_{\nu\sigma} + 2$ in equation (33). Clearly, $n_{\nu\sigma} + 1 = 0$ produces no absorption, since this means that there are no atoms in the initial state. When the equations are developed along similar lines as before, we get

$$w_{abs} = \frac{\omega_\nu^3 g_2}{4\pi^2 \varepsilon_o \hbar c^3} \left(\frac{\varepsilon}{\varepsilon_o}\right)^{\frac{1}{2}} \bar{n}_{\nu\sigma} \left|\mu_{fi}^{\nu\sigma}\right|^2 d\Omega \tag{43}$$

where $\bar{n}_{\nu\sigma}$ is the average number of photons in each mode.

C. Multiple Photon Processes

In addition to single photon absorption and emission, it is possible to have multiple photon processes. It is necessary to use the second order approximation in calculating the scattering matrix to account for two-photon processes. Consequently, the mathematics becomes rather involved. A considerable simplification is achieved by considering only two radiation modes. In this case, the vector potential of the radiation field becomes

$$\vec{A} = \left(\frac{\hbar}{2\varepsilon_o V}\right)^{\frac{1}{2}} \left[\frac{\vec{e}_1}{(\omega_1)^{\frac{1}{2}}} \left(a_1^+ e^{-i\vec{k}_1 \cdot \vec{r}} + a_1 e^{i\vec{k}_1 \cdot \vec{r}}\right) + \frac{\vec{e}_2}{(\omega_2)^{\frac{1}{2}}} \left(a_2^+ e^{-i\vec{k}_1 \cdot \vec{r}} + a_2 e^{i\vec{k}_2 \cdot \vec{r}}\right) \right] \tag{44}$$

The initial and final states for two-photon absorption are

$$|E_i\rangle = |\Psi_i\rangle\ |n_1\rangle|n_2\rangle \tag{45}$$

$$|E_f\rangle = |\Psi_f\rangle\ |n_1-1\rangle\ |n_2-1\rangle \tag{46}$$

and, as usual, the interaction Hamiltonian is

$$H = -\frac{e}{m}\vec{p}\cdot\vec{A} \tag{47}$$

The probability of two-photon absorption is now given by

$$P_f = |\langle E_f|\ S\ |E_i\rangle|^2 \tag{48}$$

but the first order does not contribute; so, using the second order, we have

$$P_f = \left|\langle E_f|\ \frac{1}{(i\hbar)^2}\int_0^t d\tau_1 \int_0^{\tau_1} H'_{int}(\tau_1)\, H'_{int}(\tau_2)\, d\tau_2\ |E_i\rangle\right|^2 \tag{49}$$

Using steps similar to those we used to find the first order probability, and inserting the operator

$$I = \sum_\nu |E_\nu\rangle\langle E_\nu| \tag{50}$$

where the $|E_\nu\rangle$vectors form a complete set of eigenvectors for H_o, we have

$$P_f = \left| \frac{1}{(i\hbar)^2}\sum_\nu \{\langle E_f|\ H_{int}\ |E_\nu\rangle\langle E_\nu|\ H_{int}\ |E_i\rangle \int_0^t d\tau_1 \int_0^{\tau_1} e^{i(E_f - E_\nu)\frac{\tau_1}{\hbar}}\, e^{i(E_\nu - E_i)\frac{\tau_2}{\hbar}}\, d\tau_2\ \}\right|^2 \tag{51}$$

This can be integrated to give

$$P_f = \left| -2i\sum_\nu \{\frac{\langle E_f\ H_{int}\ E_\nu\rangle\langle E_\nu\ H_{int}\ E_i\rangle}{E_i - E_\nu}\ e^{i(E_f - E_\nu)\frac{t}{2\hbar}}\ \frac{\sin(E_i - E_f)\frac{t}{2\hbar}}{E_i - E_f}\ \}\right|^2 \tag{52}$$

Here we have neglected the quantity

$$\int_0^t e^{i(E_f - E_\nu)\frac{\tau_1}{\hbar}} d\tau_1 = \int_0^t e^{i\omega\tau_1} d\tau_1 \tag{53}$$

because it is a rapidly oscillating function of t, and hence, gives a negligible contribution to the total integral. The transition probability per unit time is, accordingly,

$$w = \frac{dP}{dt} = \frac{d}{dt}\int P_f N\rho dE_f = \frac{2\pi}{\hbar}\left|\sum_\nu\left\{\frac{\langle E_f|H_{int}|E_\nu\rangle\ \langle E_\nu|H_{int}|E_i\rangle}{E_i - E_\nu}\right\}\right|^2 N\rho \tag{54}$$

where N is the number of atoms and ρ is their energy density.

If we now insert the terms for H_{int} and $\vec{A}$, we obtain the following result:

$$w = \frac{\pi\hbar}{2\varepsilon_o{}^2V^2}\frac{n_1 n_2}{\omega_1\omega_2}\left(\frac{e}{m}\right)^4 N\rho\left|\sum_\nu\left\{\frac{\langle\Psi_f|\ \vec{e}_2\cdot\vec{p}\ |\Psi_\nu\rangle\ \langle\Psi_\nu|\ \vec{e}_1\cdot\vec{p}\ |\Psi_i\rangle}{W_i - W_\nu + \hbar\omega_1} + \frac{\langle\Psi_f|\ \vec{e}_1\cdot\vec{p}|\Psi_\nu\rangle\ \langle\Psi_\nu|\ \vec{e}_2\cdot\vec{p}\ |\Psi_i\rangle}{W_i - W_\nu + \hbar\omega_2}\right\}\right|^2 \tag{55}$$

where the Ψ's are electron wave functions, and the W's are the corresponding energy eigenvalues. Here it is assumed that $e^{i\vec{k}\cdot\vec{r}}$ is constant over the range where Ψ gives an appreciable contribution to the integrand.

Two-photon absorption can be interpreted as the absorption of one photon, which raises the system to a virtual state Ψ_ν, together with the simultaneous absorption of a second photon, which raises the system to the final state, Ψ_f.

If there is only one radiation mode so that $\omega_1 = \omega_2$, then we get

$$w = \frac{\pi\hbar}{2\varepsilon_o{}^2V^2}\frac{n(n-1)}{\omega^2}\left(\frac{e}{m}\right)^4 N\rho\left|\sum_\nu\left\{\frac{\langle\Psi_f|\ \vec{e}\cdot\vec{p}\ |\Psi_\nu\rangle\ \langle\Psi_\nu|\ \vec{e}\cdot\vec{p}\ |\Psi_i\rangle}{W_i - W_\nu + \hbar\omega}\right\}\right|^2 \tag{56}$$

It is interesting to note that even though the probability for two-photon processes is much lower than for single photon processes, the probability is proportional to n^2; that is, the transition probability is proportional to the intensity of the light squared, whereas single photon processes are linearly dependent on the intensity. This is the reason that higher order processes come into importance when light from high-powered Q-switched lasers is passed through matter.

By now, it should be clear that probabilities for three-photon and higher order absorption can be calculated by using higher orders of the scattering matrix. Clearly, multiple-photon emission is also a possible process in this regime of high-power radiation fields.

D. Raman Scattering

The literature on Raman scattering is amazing from the standpoint of ways in which the theory is treated. These range from a quantum mechanical second order perturbation theory through a semiclassical third order perturbation theory to a strictly classical treatment. Each of the different methods have value, so we will briefly examine two of them.

From a classical point of view, we can account for Raman scattering in the following way. Consider a molecule as consisting of an electron cloud surrounding the nuclei. Further, let the incident radiation on the molecule be represented by a monochromatic wave whose

electric vector at the position of the molecule is given by

$$E = E_o \sin \omega_p t \tag{57}$$

The polarization produced by such a field is

$$|P| = \alpha|E| \tag{58}$$

where α is called the polarizability of the molecule. This polarization is due to the positive nuclei moving one direction under the influence of the field E, while the electron cloud is displaced slightly the other direction. Under the influence of visible or ultraviolet light, the frequency is so great that the heavy nuclei cannot respond; hence, the polarization is due almost entirely to the movement of the electron cloud.

If the nuclei are vibrating, it is obvious that this will affect the polarizability of the molecule slightly, due to the change of the relative positions of the nuclei and electron cloud. To a first approximation, we can account for this change by writing

$$\alpha = \alpha_o + \alpha \cdot \sin \omega_\upsilon t \tag{59}$$

where $\alpha_o >> \alpha$ and ω_υ is the frequency of vibration of the molecule. Using this value of the polarizability we get

$$P = \alpha_o E_o \sin \omega_p t + \alpha_1 E_o \sin \omega_\upsilon t \sin \omega_p t \tag{60}$$

Using trigonometric identities, this can be rewritten

$$P = \alpha_o E_o \sin\omega_p t + \tfrac{1}{2}\alpha_1 \cos(\omega_p - \omega_\nu)t - \tfrac{1}{2}\alpha_1 \cos(\omega_p + \omega_\nu)t \qquad (61)$$

The oscillating polarization classically gives rise to radiation at the frequencies of the polarization which are: ω_p, corresponding to Rayleigh scattering; $(\omega_p - \omega_\upsilon)$, corresponding to Stokes Raman scattering; and $(\omega_p + \omega_\upsilon)$, corresponding to anti-Stokes Raman scattering.

The drawbacks to this simple-minded treatment are several. It predicts the Stokes and anti-Stokes lines will be of equal intensity. It doesn't predict rotational or electronic Raman scattering, and it doesn't predict more than the first order lines, although from a classical point of view, one would suspect that all of the "beat" frequencies of ω_p and ω_υ would be present. The classical point of view really isn't very satisfactory.

Using much of the same procedure as was used in two-photon absorption, we can calculate the probability for Raman scattering by using the second order approximation of the scattering operator. For the interaction Hamiltonian, we will use

$$H_{int} = -\frac{e}{m}(\vec{p} \cdot \vec{A}) \qquad (62)$$

and the initial and final states will be

$$|E_i\rangle = |\Psi_i\rangle\,|n_p\rangle|n_r\rangle \qquad (63)$$

$$|E_f\rangle = |\Psi_f\rangle \; |n_p - 1\rangle \; |n_r + 1\rangle \tag{64}$$

where n_p is the number of photons in the primary mode, and n_r is the number in the Raman mode.

The e and $\vec{p}$ in the interaction Hamiltonian refer to the charge and momentum operator of charged particles in the molecule doing the scattering. We will omit the sum over all particles for simplicity, and remember that it might be an electron or a nucleus. The scattering could give rise to the change of electronic, rotational, or vibrational state of the molecule. It most frequently results in a change of vibrational state.

Performing the calculations as before, we obtain

$$w = \frac{\pi \hbar}{2\varepsilon_p \varepsilon_r V^2} \frac{n_p(n_r + 1)}{\omega_p \omega_r} \left(\frac{e}{m}\right)^4 N_i \rho \left| \sum_\nu \left\{ \frac{\langle \Psi_f | \vec{e}_r \cdot \vec{p} \; | \Psi_\nu \rangle \; \langle \Psi_\nu | \vec{e}_p \cdot \vec{p} \; | \Psi_i \rangle}{W_i - W_\nu + \hbar\omega_p} \right.\right. \left.\left. \frac{\langle \Psi_f | \vec{e}_p \cdot \vec{p} \; | \Psi_\nu \rangle \; \langle \Psi_\nu | \vec{e}_r \cdot \vec{p} \; | \Psi_i \rangle}{W_i - W_\nu - \hbar\omega_r} \right\} \right|^2 \tag{65}$$

For this process, N_i is the total number of molecules in the initial state, and ρ is the energy difference distribution function for the final and initial states.

This transition probability is actually for the Stokes part of Raman scattering, i.e., $W_f > W_i$. We can obtain the anti-Stokes part by interchanging the indices p and r, and then, since we want to use the same two eigenstates of the molecule, we interchange the indices i and f. Now, using the conservation of energy

$$W_f - W_i = \hbar(\omega_p - \omega_r) \tag{66}$$

we note that the term inside the absolute value signs for anti-Stokes scattering is just the complex conjugate of the value for Stokes scattering. When the absolute value is taken they are the same.

The total transition probability per unit time, which amounts to emission of a photon at ω_r, is the probability for Stokes scattering with a transition from Ψ_i to Ψ_f, minus the probability for anti-Stokes scattering with a transition from Ψ_f to Ψ_i.

The total transition probability per unit time is

$$w = \frac{\pi\hbar}{2\varepsilon_p \varepsilon_r V^2} \left(\frac{e}{m}\right)^4 \frac{\rho}{\omega_p \omega_r} \left[N_i n_p (n_r+1) - N_f n_r (n_p+1)\right] \left| \sum_\nu \left\{ \frac{\langle \Psi_f | \vec{e}_r \cdot \vec{p} | \Psi_\nu \rangle \langle \Psi_\nu | \vec{e}_p \cdot \vec{p} | \Psi_i \rangle}{W_i - W_\nu + \hbar\omega_p} + \frac{\langle \Psi_f | \vec{e}_p \cdot \vec{p} | \Psi_\nu \rangle \langle \Psi_\nu | \vec{e}_r \cdot \vec{p} | \Psi_i \rangle}{W_i - W_\nu - \hbar\omega_r} \right\} \right|^2 \tag{67}$$

The total power scattered into dq radiation modes in the frequency interval $d\omega r$ and solid angle $d\Omega$ is

$$\Delta P = \int_o^\infty w \hbar\omega_r \frac{dq}{d\omega_r} \, d\omega_r \tag{68}$$

The number of radiation modes of one polarization is given by

$$dq = \frac{V}{(2\pi)^3} k_r^2 dk_r d\Omega = \frac{V}{(2\pi)^3} \frac{\omega_r^2}{c^3} \left(\frac{\varepsilon_r}{\varepsilon_o}\right)^{\frac{3}{2}} d\omega_r d\Omega \tag{69}$$

If we now make use of the fact that the energy difference distribution function, ρ, is normalized according to the following condition

$$\int \rho(W_f - W_i) \, d(W_f - W_i) = \hbar \int_o^\infty \rho(\hbar\omega_p - \hbar\omega_r) \, d\omega_r = 1 \tag{70}$$

and also ρ is narrow enough to consider all other factors constant in the range where it has appreciable value, we can obtain

$$\Delta P = \frac{\hbar\omega_r^{\,2}}{(4\pi\varepsilon_o)^2\, V\, \omega_p \varepsilon_p} \left(\frac{e}{mc}\right)^4 \left[N_i n_p (n_r + 1) - N_f n_r (n_p + 1) \right] \tag{71}$$

$$\left| \sum_{\nu} \left\{ \frac{\langle \Psi_f | \vec{e}_r \cdot \vec{p} | \Psi_\nu \rangle \langle \Psi_\nu | \vec{e}_p \cdot \vec{p} | \Psi_i \rangle}{W_i - W_\nu + \hbar\omega_p} + \frac{\langle \Psi_f | \vec{e}_p \cdot \vec{p} | \Psi_\nu \rangle \langle \Psi_\nu | \vec{e}_r \cdot \vec{p} | \Psi_i \rangle}{W_i - W_\nu - \hbar\omega_r} \right\} \right|^2$$

The incident power per unit area is

$$S_i = \hbar\omega p \frac{n_p}{V} \left(\frac{\varepsilon_o}{\varepsilon_p}\right)^{1/2} c \tag{72}$$

If we set $n_r = 0$ and take $\frac{\Delta P}{S_i}$ we can obtain the ratio of the spontaneously scattered Raman power in a solid angle, $d\Omega$, to the incident power flux.

$$\frac{\Delta P}{S_i} = \frac{1}{(4\pi\varepsilon_o)^2} \left(\frac{\varepsilon_r}{\varepsilon_p}\right) \left(\frac{\omega_r}{\omega_p}\right)^2 \left(\frac{e}{mc}\right)^4 N_i \left| \sum_{\nu} \ldots\ldots \right|^2 d\Omega = \sigma d\Omega \tag{73}$$

The quantity σ, as introduced, is the cross section for spontaneous Raman scattering. It is a value which can be measured in the laboratory.

The momentum operator in the equations for W and σ can be replaced by the dipole moment by following the same procedure as before. The result is

$$\sigma = \frac{1}{(4\pi\varepsilon_o)^2} \left(\frac{\varepsilon_r}{\varepsilon_p}\right)^{1/2} \left(\frac{\omega_r}{c}\right)^4 N_i \left| \sum_{\nu} \left\{ \frac{\langle \Psi_f | \vec{e}_r \cdot \vec{\mu} | \Psi_\nu \rangle \langle \Psi_\nu | \vec{e}_p \cdot \vec{\mu} | \Psi_i \rangle}{W_f - W_i + \hbar\omega_r} + \frac{\langle \Psi_f | \vec{e}_p \cdot \vec{\mu} | \Psi_\nu \rangle \langle \Psi_\nu | \vec{e}_r \cdot \vec{\mu} | \Psi_i \rangle}{W_i - W_\nu - \hbar\omega_r} \right\} \right|^2 \tag{74}$$

E. Rayleigh Scattering

There is an interesting two-photon process which involves simultaneous absorption of a photon in one mode and emission into another mode, where the two photons are of the same frequency or at least differ in frequency by no more than the Doppler frequency. This process is the well known Rayleigh scattering.

To solve for the transition probability, we will use the scattering operator to second order and will use the interaction Hamiltonian in the form

$$H_{int} = -\frac{e}{m}(\vec{p}\cdot\vec{A}) + \frac{e^2}{2m}\vec{A}^2 \tag{75}$$

The $\vec{A}^2$ term is negligible in the second order part of the scattering operator, and the $\vec{p}\cdot\vec{A}$ term is zero in the first order part. The only terms we are concerned with then in S are

$$S = \frac{1}{i\hbar}\int_0^t e^{\frac{iH_o\tau}{\hbar}}\frac{e^2}{2m}\vec{A}^2 e^{-\frac{iH_o\tau}{\hbar}}d\tau + \tag{76}$$

$$\frac{1}{(i\hbar)^2}\int_0^t d\tau_1\int_0^{\tau_1} e^{-\frac{iH_o\tau_1}{\hbar}}(\vec{p}\cdot\vec{A})\, e^{-\frac{iH_o\tau_1}{\hbar}} e^{\frac{iH_o\tau_2}{\hbar}}(\vec{p}\cdot\vec{A})\, e^{-\frac{iH_o\tau_2}{\hbar}}d\tau_2$$

The probability for transition from $|E_f\rangle$ to $|E_i\rangle$ will be

$$P_f = |\langle E_f|\ S\ |E_i\rangle|^2 \tag{77}$$

where, for this case,

$$|E_i\rangle = |\Psi_i\rangle\ |n_1\rangle\ |n_2\rangle \tag{78}$$

$$|E_f\rangle = |\Psi_i\rangle\ |n_1 - 1\rangle\ |n_2 + 1\rangle \tag{79}$$

Following the same procedures as we have used on the earlier derivation, we obtain

$$w = \frac{dP}{dt} = \frac{d}{dt} \int P_f \rho dE_f =$$

$$\frac{V\omega^2}{4\pi^2\hbar^2c^3}\left(\frac{e}{m}\right)^4 \left| \sum_n \left\{ \sum_\nu \left(\frac{\langle E_f|\vec{p}_n \cdot \vec{A}_n|E_\nu\rangle\ \langle E_\nu|\vec{p}_n \cdot \vec{A}_n|E_i\rangle}{E_i - E_\nu} \right) \right.\right. \tag{80}$$

$$\left.\left. + \frac{m}{2}\ \langle E_f|\vec{A}_n^2|E_i\rangle \right\} \right|^2 d\Omega$$

The sum over n is taken to account for the extension of the theory from one scattering atom to a gas containing many atoms. Choosing the density of final states as we have makes our result valid only for the case where the mode receiving the scattered radiation was empty before the scattering process. This is the only case we can calculate using energy eigenstates. Other cases involve phase information of the radiation which we do not have when using energy eigenstates.

If we now consider only two radiation modes the vector potential becomes

$$\vec{A}_n = \left(\frac{\hbar}{2\varepsilon_o V\omega}\right)^{\frac{1}{2}} \left[\vec{e}_1 \left(a_1^+ e^{-i\vec{k}_1\cdot\vec{r}_n} + a_2 e^{i\vec{k}_1\cdot\vec{r}_n}\right) + \vec{e}_2 \left(a_2^+ e^{-i\vec{k}_2\cdot\vec{r}_n} + a_2 e^{i\vec{k}_2\cdot\vec{r}_n}\right) \right] \tag{81}$$

Assuming that all of the gas atoms are identical, which means $\vec{p}$ is independent of n, we can enter the vector potential into equation (80) to obtain

$$w = \frac{\omega^2 n_1 c}{(4\pi\varepsilon_o)^2 V} \left(\frac{e}{mc}\right)^4 \left| \left\{ \sum_\nu \left(\frac{\langle\Psi_f|\vec{e}_1\cdot\vec{p}|\Psi_\nu\rangle \langle\Psi_\nu|\vec{e}_2\cdot\vec{p}|\Psi_i\rangle}{W_i - W_\nu - \hbar\omega} + \frac{\langle\Psi_f|\vec{e}_2\cdot\vec{p}|\Psi_\nu\rangle \langle\Psi_\nu|\vec{e}_1\cdot\vec{p}|\Psi_i\rangle}{W_i - W_\nu + \hbar\omega} \right) + m(\vec{e}_1\cdot\vec{e}_2) \right\} \sum_n e^{-i(\vec{k}_2 - \vec{k}_1)\cdot\vec{r}_n} \right|^2 d\Omega \tag{82}$$

If we assume that the scattering atoms are randomly distributed, then

$$\left| \sum_n e^{-i(\vec{k}_2 - \vec{k}_1)\cdot\vec{r}_n} \right|^2 = \begin{cases} NV & \vec{k}_2 \neq \vec{k}_1 \\ (NV)^2 & \vec{k}_2 = \vec{k}_1 \end{cases} \tag{83}$$

where N is the number of scattering atoms per unit volume. In other words, forward scattering occurs much more strongly than in any other direction. We can use this knowledge to calculate the power scattering out of the incident beam. Since W is the number of photons scattered per unit time, then the power scattered out of the beam, P_s, is

$$P_s = w\hbar\omega \tag{84}$$

The incident power is

$$P_i = \hbar\omega n_1 \frac{c}{L} \tag{85}$$

where L is the length of the scattering path. The ratio then is

$$\frac{P_s}{P_i} = \frac{wL}{n_1 c} = \frac{NL}{(4\pi\varepsilon_o)^2}\left(\frac{e}{mc}\right)^4 \left| \sum_{\nu} \left(\frac{\langle \Psi_i | \vec{e}_1 \cdot \vec{p} | \Psi_\nu \rangle \langle \Psi_\nu | \vec{e}_2 \cdot \vec{p} | \Psi_i \rangle}{W_i - W_\nu + \hbar\omega} + \right.\right. \tag{86}$$

$$\left.\left. \frac{\langle \Psi_i | \vec{e}_2 \cdot \vec{p} | \Psi_\nu \rangle \langle \Psi_\nu | \vec{e}_1 \cdot \vec{p} | \Psi_i \rangle}{W_i - W_\nu + \hbar\omega} \right) + m(\vec{e}_1 \cdot \vec{e}_2) \right|^2 d\Omega$$

This can also be written in the equivalent manner using the dipole moment operator instead of the momentum operator. Namely

$$\frac{P_s}{P_i} = \frac{NL}{(4\pi\varepsilon_o)^2}\left(\frac{\omega}{c}\right)^4 \left| \sum_{\nu} \left(\frac{\langle \Psi_i | \vec{e}_1 \cdot \vec{\mu} | \Psi_\nu \rangle \langle \Psi_\nu | \vec{e}_2 \cdot \vec{\mu} | \Psi_i \rangle}{W_i - W_\nu - \hbar\omega} + \right.\right. \tag{87}$$

$$\left.\left. \frac{\langle \Psi_i | \vec{e}_2 \cdot \vec{\mu} | \Psi_\nu \rangle \langle \Psi_\nu | \vec{e}_1 \cdot \vec{\mu} | \Psi_i \rangle}{W_i - W_\nu + \hbar\omega} \right) \right|^2 d\Omega$$

This can also be expressed in terms of the index of refraction for an isotropic gas

$$\frac{P_s}{P_i} = \frac{\omega^4 L}{(4\pi)^2 c^4 N} (\vec{e}_1 \cdot \vec{e}_2)(n^2 - 1)^2 \, d\Omega \tag{88}$$

When integration is performed over all possible polarizations and all directions, the ratio of power scattered per unit length to incident power becomes

$$\frac{P_s}{LP_i} = \frac{\omega^4}{6\pi\, Nc^4} (n^2 - 1)^2 \tag{89}$$

$$\approx \frac{2\omega^4}{3\pi Nc^4} (n - 1)^2 \text{ for } (n - 1) << 1$$

Summarizing, briefly, we note that some of the effects we can account for by using this method of treating Rayleigh scattering are: (1) that the scattering is primarily in the forward direction; (2) it depends on the fourth power of the frequency; (3) there is a relationship between scattered power and relative orientation of polarization of the incident and scattered wave; and (4) the Rayleigh scattering peaks strongly near allowed dipole transition frequencies.

F. Brillouin Scattering

The scattering of light by sound waves was first considered by Brillouin[12] in 1922. The effect takes place in liquids and solids. Recently, some results of stimulated scattering were even observed in gases under high pressure.[13] The quantum mechanical description of Brillouin scattering is much too involved to treat here, and is of little interest in relation to the experiment performed. The quantum mechanical development is made, however, by considering the interaction of accoustical phonons with photons. The classical treatment as presented by Yariv[14] is too long to include; but we will use some of his results to discuss stimulated Brillouin scattering.

Fortunately, Yariv has also shown that from a phenomenological point of view, Brillouin scattering can be treated in a very simple manner. Consider a sound wave, with frequency ω_s, wavelength λ_s, and wave vector $\vec{k}_s$, traveling through a medium. The wave will consist of moving regions of compression and rarefaction which will give rise to corresponding variations in the dielectric constant, and hence, the index of refraction. The variation in index of refraction will cause a partial reflection of light incident at some angle, α, to the plane of the wave front as shown in Figure 1. The result is somewhat analogous to reflection of light from a grating or X-rays from a crystal. The condition for reflection is

$$2\lambda_s \sin \alpha = \lambda_L \qquad \text{(first order)} \tag{90}$$

The subscript s is for the sound wave, L for the incident light, and b is for the scattered light.

In addition to being reflected, the light is Doppler shifted because of the movement of the sound wave. Assuming the velocity of the sound wave, υ_s, is very much smaller than the velocity of the light wave, υ_L, this Doppler shift is

$$\omega_b = \omega_L \left(1 - \frac{2\,\upsilon_s \sin \alpha}{\upsilon_L}\right) \tag{91}$$

Combining the two equations, we obtain the relation

$$\omega_b = \omega_L - \omega_s \tag{92}$$

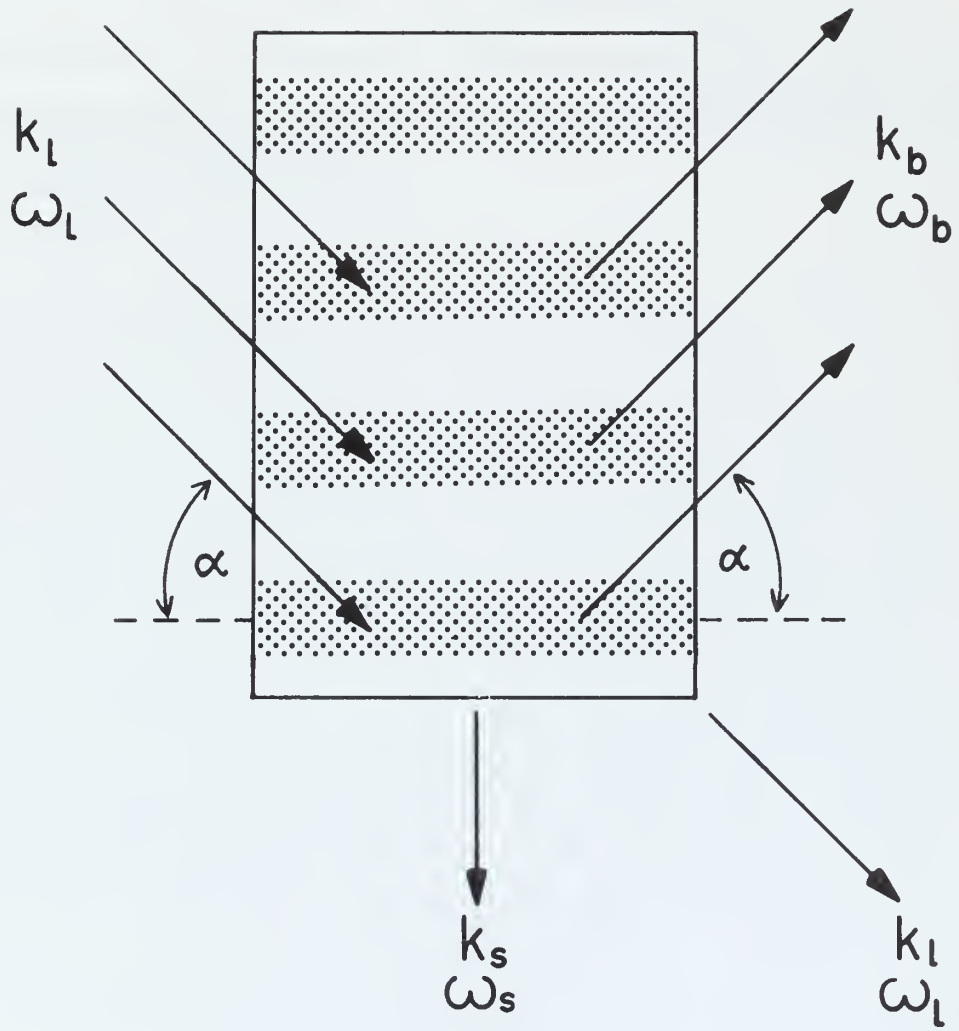

FIGURE 1. Brillouin Scattering

which is, of course, a statement of conservation of energy.

Conservation of momentum would require that

$$\vec{k}_b = \vec{k}_L - \vec{k}_s \tag{92a}$$

which gives the Bragg reflection condition when $v_s << v_L$.

For a receding sound wave, the light pressure would be feeding energy into the accoustical wave. After giving up part of its energy, the frequency of the light wave reflected is given by equation (92). Though this description is neither complete nor accurate, it does illustrate the phenomenon taking place.

III. STIMULATED PROCESSES

A. Stimulated Emission

So far in this paper, we have limited our discussion to spontaneous processes, except for absorption, which can never take place spontaneously. All of the spontaneous processes mentioned can also take place as stimulated processes. That is, the probability of a photon being emitted into a mode, $\nu\sigma$, is influenced by the number of photons, $n_{\nu\sigma}$, already present in that mode. Wherever the factor $(n_{\nu\sigma} + 1)$ has occurred, we have set $n_{\nu\sigma} = 0$ for spontaneous processes. So now we will set the number of photons equal to $n_{\nu\sigma} + 1$ for stimulated processes.

The first process we will deal with is stimulated emission. Equation (23) gave the probability of a transition from state $|E_i\rangle$ to state $|E_f\rangle$. For spontaneous emission, we considered the electronic states $|\Psi_i\rangle$ and $|\Psi_f\rangle$ to have fixed energies, W_i and W_f, and considered the density of final states to be the density of photon states available. For stimulated emission, the mode into which the photons are emitted is also fixed, however, so the probability is

$$P = \frac{2\pi t}{\hbar} |\langle E_f| H_{int} |E_i\rangle|^2 \delta(E_f - E_i) \tag{93}$$

The quantity $|\langle E_f| H_{int} |E_i\rangle|$ can be evaluated in the same manner as was employed for the case of spontaneous emission. This gives

$$P_{ste} = t \frac{\pi \omega_\nu}{\varepsilon V} n_{\nu\sigma} |\bar{\mu}_{fi}|^2 g_i \delta(E_f - E_i) \tag{94}$$

We have used $|\bar{\mu}_{fi}|^2$ as the average value over all possible orientations of the system involved.

This is the probability of emission from one particular atom. If we want the total probability of emission,we must sum over all of the atoms. Owing to Doppler shifts and external perturbations, not all atoms have eigenstates of exactly the same energy difference, $W_i - W_f$, so we assume an energy distribution of the form

$$dN = N_2 \rho(W_i - W_f)\, d(W_i - W_f) \tag{95}$$

where dN is the fractional number of atoms of energy difference $W_i - W_f$ in the interval $d(W_i - W_f)$. N^2 is the total number of atoms of energy W_i and $\rho(W_i - W_f)$ is the distribution function normalized such that

$$\int_0^\infty \rho(W_i - W_f)\, d(W_i - W_f) = 1 \tag{96}$$

Using this we get

$$p = \sum_n P_{ste} \tag{97}$$

and if we approximate the sum with an integral, we obtain

$$P = \int t \frac{\pi\omega_\nu}{\varepsilon V} n_{\nu\sigma} |\bar{\mu}_{fi}|^2 g_1 \delta(E_f - E_i) N_2 \rho(W_i - W_f)\, d(W_i - W_f) \tag{98}$$

We have already stipulated that the photon energies are fixed so that

$$d(W_i - W_f) = d(E_i - E_f) \tag{99}$$

and the delta function then serves to fix the value of $W_i - W_f$ at

$$W_i - W_f = \hbar\omega_\nu \tag{100}$$

The net probability per unit time for stimulated emission then is

$$w_{ste} = \frac{dP}{dt} = \frac{\pi\omega_\nu}{\varepsilon V} n_{\nu\sigma} N_2 g_1 \rho(\hbar\omega_\nu) \quad |\bar{\mu}_{fi}|^2 \tag{101}$$

The calculation of absorption probability per unit time from a given mode, $\nu\sigma$, proceeds in the same manner as the emission calculation, except we use N_1, the number of atoms in the lower level, and g_2, the degeneracy of the upper level. The result is

$$w_{abs} = \frac{\pi\omega_\nu}{\varepsilon V} n_{\nu\sigma} N_1 g_2 \rho(\hbar\omega_\nu) \ |\bar{\mu}_{if}|^2 \tag{102}$$

The power in the mode $\nu\sigma$ changes by the amount

$$\Delta P = (w_{ste} - w_{abs}) \hbar\omega_\nu \tag{103}$$

We should note here that $|\bar{\mu}_{fi}| = |\bar{\mu}_{if}|$. This follows from the Hermitean properties of the dipole moment operator. Hence,

$$\Delta P = \frac{\hbar\pi\omega_\nu}{\varepsilon V} n_{\nu\sigma} \rho(\hbar\omega_\nu) \left[N_2 g_1 - N_1 g_2 \right] |\bar{\mu}_{fi}|^2 \tag{104}$$

At this point, it is convenient to define a quantity α, the relative

power gain per unit length

$$\alpha = \frac{\Delta P}{P_i L} \tag{105}$$

P_i is the power in mode $\nu\sigma$ and L is the length of the cavity, so

$$P_i = \frac{n\nu\sigma}{L} \hbar\omega_\nu \left(\frac{\varepsilon_o}{\varepsilon}\right)^{\frac{1}{2}} c \tag{106}$$

If we also define the number of atoms per unit volume as

$$N_1 = \frac{N_1}{V} \qquad N_2 = \frac{N_2}{V} \tag{107}$$

then we can write

$$\alpha = \frac{\pi\omega_\nu}{(\varepsilon\varepsilon_o)^{\frac{1}{2}} c} \rho(\hbar\omega_\nu) \left[N_2 g_1 - N_1 g_2\right] |\bar{\mu}_{fi}|^2 \tag{108}$$

It is possible to use equation (42) to express $|\bar{\mu}_{fi}|$ in terms of the spontaneous radiation lifetime. We can also use the normalization condition to relate the energy distribution function, $\rho(\hbar\omega_\nu)$, to the frequency distribution function $\rho'(\nu)$:

$$\int_o^\infty \rho(\hbar\omega_\nu)\hbar d\omega_\nu = \int_o^\infty \rho'(\nu)d\nu = 1 \tag{109}$$

but

$$\omega_\nu = 2\pi\nu \tag{110}$$

so

$$\rho(\hbar\omega_\nu) = \frac{1}{2\pi\hbar} \rho'(\nu) \tag{111}$$

This enables us to write

$$\alpha = \frac{c^2\varepsilon_o}{8\pi\varepsilon\nu^2\tau_{spe}}\left[N_2 - \frac{g_2}{g_1}N_1\right]\rho'(\nu) \qquad (112)$$

This is the expression commonly used in the literature where $\frac{\varepsilon}{\varepsilon_o}$ is expressed as the square of the index of refraction. When there is a population inversion, (that is, when $N_2 > \frac{g_2}{g_1}N_1$), then $\alpha > 0$ and the field gains power by stimulated emission. If, as is generally the case, $N_2 < \frac{g_2}{g_1}N_1$, then power is lost through absorption.

B. Stimulated Raman Scattering

We have previously stated that any light scattering process can be a stimulated process if the energy entering the scattered mode per unit length of scatterer exceeds the energy lost. The stimulated Raman effect was first observed by Woodbury and Ng,[15] and identified by Eckhardt, et al,[3] in nitrobenzene. It has since been observed and studied in many other materials. We will develop here only a very simple description of the process.

In equation (67), we calculated the probability per unit time for Raman scattering into a given mode. If we divide this probability by the length of the scattering medium we get the number of photons scattered per unit time into the Raman mode:

$$\Delta n = \frac{W}{L}$$

The gain coefficient, α, is then obtained by dividing Δn by the incident Raman flux per unit area, n. The result is

$$n = \frac{n_r}{L} \left(\frac{\varepsilon_o}{\varepsilon_r}\right)^{\frac{1}{2}} c$$

$$\alpha = \frac{\Delta n}{n} = \frac{\pi \hbar c^3 n_p \rho}{2\, \varepsilon_p (\varepsilon_r \varepsilon_o)^{\frac{1}{2}} V^2 \omega_p \omega_r} \left(\frac{e}{mc}\right)^4 \left[N_i - N_f\right] |\Sigma \ldots|^2 \tag{113}$$

We have neglected spontaneous scattering by assuming $n_p \simeq n_p + 1$ and $n_r \simeq n_r + 1$

Using the definitions of incident power and of the cross section for spontaneous Raman scattering as given by equations (72) and (73), and using the number of atoms per unit volume $N_i = \frac{N_i}{V}$ and $N_f = \frac{N_f}{V}$, we can express α in the form

$$\alpha = 8\pi^3 \frac{\varepsilon_o\, c^3\, \rho\, \sigma}{\varepsilon_r\, \omega_r^3\, V} S_i \frac{N_i - N_f}{N_i} \tag{114}$$

This relation gives us a method of calculating the gain of a Raman laser by measuring the input power flux, S_i, and the spontaneous Raman scattering cross section per unit volume in a given direction, $\frac{\sigma}{V}$. The gain coefficient, α, is very small except when the incident power, S_i, is extremely large,as it is in Q-switched lasers.

For thermal equilibrium and Stokes scattering, $N_i > N_f$ so $\alpha > 0$ and we have gain into the Stokes mode. For anti-Stokes scattering, $N_f > N_i$ so $\alpha > 0$ and there is a loss in the anti-Stokes mode. Our theory thus predicts gain for the Stokes mode and loss for the anti-Stokes mode. Terhune,[16] however, has observed stimulated anti-Stokes radiation, which is contrary to the predictions of the above theory.

A number of investigators have reported differences between experiment and the simple theory outlined above. However, Bloembergen[17] and Lallemand[18] have stated that the differences may be due to the fact that in many experiments the stimulated Raman effect cannot be separated from other "nonlinear" effects such as self-focusing of light, stimulated Rayleigh scattering, stimulated Brillouin scattering, and scattering of light by light.

The simple theory does give a means of calculating approximately the gain for most substances. For hydrogen gas at low pressures (less than 10 atm.), Bret and Denariez[19] have indicated that the theory is qualitatively correct. It is probably fair to assume that the theory is useful for most diatomic gases at low pressures.

Thus far in the discussion of Raman scattering, we have not specifically mentioned the process in crystals. There is a good reason for this. The theory of Raman scattering in solids is quite involved, and the experiments reported herein did not include crystals. However, in passing, it may be noted that Raman processes in solids involve the interaction of optical phonons with the incident photons.

C. Stimulated Rayleigh Scattering

In Chapter II, the theory of Rayleigh scattering was outlined, using energy eigenstates. However, the use of energy eigenstates does not yield information about the phase of the incident or the

scattered radiation. This lack of phase information precludes a direct calculation of Rayleigh scattering along the same lines as the above theory.

Fortunately, Mash, et al,[20] have suggested a classical solution to the problem. They suggest solving simultaneously the non-linear Maxwell's equations and the non-linear equations for the anisotropy tensor of the medium. This is a formidable task, however, so we will mention here only the results obtained for threshold. This condition is

$$E^2 \geq \frac{45\ n\ k_\omega\ kT}{2\ |k_1|\ \frac{\partial \varepsilon}{\partial S}\ \frac{I(\Omega)}{I(0)}\ \Omega\tau(\alpha_1 - \alpha_2)} \tag{115}$$

E is the amplitude of the electric vector of the incident light wave, n is the index of refraction, k_ω is a composite coefficient characterizing optical losses, k is Boltzmann's constant, T is the absolute temperature, k_1 is the wave number of the Stokes component of the wing of the Rayleigh line, ε is the dielectric constant, S is the anisotropy tensor, $I(\Omega)/I(0)$ is the ratio of the intensity at the frequency Ω to the intensity at the maximum of the Rayleigh-line wing, Ω is the frequency measured from the maximum of the wing, α_1 and α_2 are the principle polarizabilities of the molecule in the medium, and τ is the anisotropy relaxation time.

D. Stimulated Brillouin Scattering

In the section on Brillouin scattering, it was mentioned that

Yariv[14] had given a classical treatment of stimulated Brillouin scattering. His calculations were made by writing the equations of motion of a volume element in a liquid or solid moving under the influence of an electric field. This classical treatment involves the idea of an electrostrictive force caused by the change in the dielectric constant induced by strain in the medium. The electric field is assumed to be the superposition of two plane waves traveling in arbitrary directions, and the solution to the equation of motion is assumed to be an accoustical plane wave. The result of the theory gives the threshold condition for exponential growth of the accoustic wave along with one of the electric fields, namely

$$|E|^2 \geq \frac{2\, T\, \varepsilon\, \alpha_s \lambda_s \alpha_\ell \lambda_\ell}{\pi^2 \gamma^2} \tag{116}$$

where E is the amplitude of the driving electric field, T is the bulk modulus of the material, ε is the normal dielectric constant of the material, γ is the electrostrictive coefficient, α_s and α_ℓ are the accoustic and optical attenuation constants of the material, and λ_s and λ_ℓ are the wave lengths of the accoustic and optical waves. For a material such as quartz, the threshold power flux,

$$S = c\varepsilon|E|^2 \tag{117}$$

is approximately 10^7 watts per square centimeter. This power is only available from giant pulse lasers. If we assume the equation can be extended to gasses, we see that the effect is not likely to occur unless the gas pressure is very high.

IV. MOLECULAR IODINE

A. Energy Levels

The absorption and resonance spectrums of molecular iodine have been studied extensively for the past sixty years. R. W. Wood[21,22,23] did most of the early measurements. These were made before the development of quantum mechanics. The spectrum of molecular iodine, I_2, is readily explained by the quantum theory of diatomic molecules. An extensive discussion of the theory is found in Herzberg, Spectra of Diatomic Molecules.[24] We will discuss here only a few of the most relevant results of the total theory.

For a homonuclear diatomic molecule, the Schroedinger equation is written in the form

$$\frac{\hbar^2}{2m} \sum_i \nabla_i^2 \Psi + \frac{\hbar^2}{2M} \sum_k \nabla_k^2 \Psi + (E - V)\Psi = 0 \tag{118}$$

where m and i refer to electrons, and M and k to the nuclei.

Born and Oppenheimer[25] have shown that in most cases, the wave function varies slowly with internuclear distance, and hence, that the first and second derivatives of Ψ with respect to nuclear coordinates may be neglected. When this approximation is used, one can write Ψ as a product

$$\Psi = \Psi_e (\ldots, x_i y_i z_i \ldots) \Psi_{vr} (\ldots\ldots, x_k y_k z_k, \ldots) \tag{119}$$

where Ψ_e and $\Psi_{\upsilon r}$ are solutions of

$$\sum_i \nabla_i^2 \Psi_e + \frac{2m}{\hbar^2}(E^{el} - V_e)\Psi_e = 0 \tag{120}$$

and

$$\sum_k \nabla_k^2 \Psi_{\upsilon_r} + \frac{2M}{\hbar^2}(E - E^{el} - V_n)\Psi_{\upsilon r} = 0 \tag{121}$$

Equation (120) is the Schroedinger equation for the electrons moving in the field of two fixed nuclei which have a potential energy V_e, and equation (121) is the Schroedinger equation for the two nuclei moving in a potential $E^{el} + V_n$ where V_n is the Coulomb potential.

Equation (121) is normally solved by use of the model of a vibrating rotator. The solutions for a vibrating rotator give the energy eigenvalues:

$$\begin{aligned} E_{\upsilon r} = {} & hc\left[\omega_e(\upsilon+\tfrac{1}{2}) - \omega_e x_e(\upsilon+\tfrac{1}{2})^2 + \omega_e y_e(\upsilon+\tfrac{1}{2})^3 + \omega_e z_e(\upsilon+\tfrac{1}{2})^4 + \ldots\right] \\ & + hc\{\left[B_e - \alpha_e(\upsilon+\tfrac{1}{2}) + B_e(\upsilon+\tfrac{1}{2})^2 + \gamma_e(\upsilon+\tfrac{1}{2})^3 + \ldots\right] J(J+1) \\ & - \left[D_e + B_e'(\upsilon+\tfrac{1}{2}) + \ldots\right] J^2(J+1)^2 + \ldots\} = E_\upsilon + E_r \end{aligned} \tag{122}$$

where υ is the vibrational quantum number and J is the rotational quantum number. The constants ω_e, $\omega_e x_e$, $\omega_e y_e$, $\omega_e Z_e$, B_e, α_e, β_e, γ_e, D_e, β_e', are determined experimentally by fitting the spectroscopic data, and are referred to as the spectroscopic constants.

At this point it should be noted that, since E^{el} refers to an eigenstate for fixed nuclei, it will in general be a function of the internuclear distance. V_n is also a function of the internuclear distance, so the "effective" potential, $E^{el} + V_n$, in which

the nuclei move, is a function of the internuclear distance. The molecule exists in a stable or bound state only if there is a minimum in the potential, $E^{el} + V_n$ with respect to internuclear distance. When such a minimum exists, there are solutions to equation (121) of the form of equation (122).

It is customary to consider the minimum value of $E^{el} + V_n$ in a stable state as the electronic energy, E_e, of that state. Also, since $E_{\upsilon r}$ is measured from the minimum for a vibrating rotator, the total energy of any state of a diatomic molecule can be written as the sum of electronic, vibrational, and rotational energies:

$$E = E_e + E_\upsilon + E_r \tag{123}$$

In wavenumber units this becomes

$$T = \frac{E}{hc} = T_e + G(\upsilon) + F(\upsilon J) \tag{124}$$

where

$$G(\upsilon) = \omega_e(\upsilon+\tfrac{1}{2}) - \omega_e x_e(\upsilon+\tfrac{1}{2})^2 + \omega_e y_e(\upsilon+\tfrac{1}{2})^3 + \omega_e z_e(\upsilon+\tfrac{1}{2})^4 + \ldots\ldots \tag{125}$$

and

$$F(\upsilon J) = \left[B_e - \alpha_e(\upsilon + \tfrac{1}{2}) + \ldots\right] J(J+1) + \tag{126}$$

$$\left[D_e - B_e'(\upsilon + \tfrac{1}{2}) + \ldots\right] J^2(J+1)^2 = B_\upsilon J(J+1) + D_\upsilon J^2(J+1)^2$$

The final result is that by fitting theory to spectroscopic data, it becomes possible to diagram the energy states of a diatomic molecule, and in particular iodine, as a function of internuclear distance as is shown in Figure 2.

B. Fluorescence

We have already discussed the general process of fluorescence and will now examine the particular case of iodine. When white light is passed through iodine vapor and the absorption spectrum is analysed, it is noted that there are thousands of very sharp and closely spaced absorption lines occurring in bands starting from a continuum at about 4995Å and extending beyond 6000Å. These absorption lines occur because the I_2 molecules in various vibrational and rotational states of the $X'\Sigma_g^+$ (ground) electronic state absorb the light and undergo a transition to various vibrational and rotational states of the $B^3\pi_{ou}^+$ electronic state lying above. The characteristics of the spectrum are determined by the energy levels of both the lower and upper state and by the selection rules governing dipole transitions. The relevant selection rules are $\Delta J = \pm 1$ and $\Delta \upsilon = \pm 1$ (unless an electronic transition is involved, and then no rule governs $\Delta \upsilon$).

Molecules in the $B^3\pi_{ou}^+$ state may undergo transitions between vibrational levels and/or rotational levels according to the selection rules. However, there is high probability that the molecule

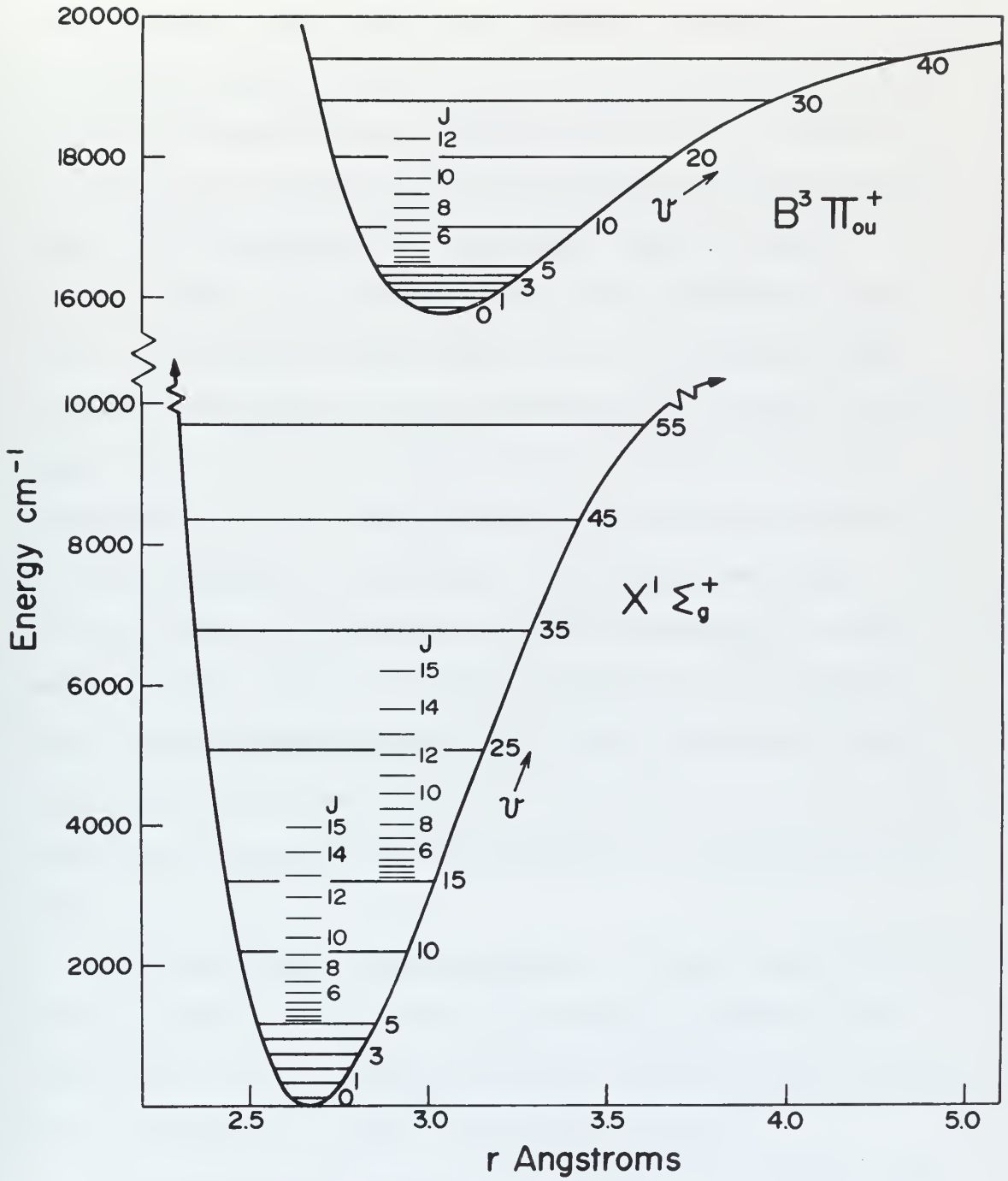

FIGURE 2. Energy Levels of Molecular Iodine
(X and B states only; rotational levels not to scale)

will return to the ground electronic state by emission of a photon (fluorescence). Since there is no selection rule involving a change of vibrational quantum number during an electronic transition, the resulting fluorescence has a spectrum as sharp and as complex as the absorption spectrum. Even when illuminated with monochromatic light, the fluorescence spectrum is highly complex because of the number of levels in the ground state to which the molecule can return. As an example, suppose light which is sufficiently monochromatic to illuminate only one absorption line is passed through iodine vapor. This will populate only one level of the B state. Suppose also that the B state decays back to the X state before the molecule undergoes any vibrational or rotational transitions. This will give rise to a fluorescence spectrum consisting of a series of pairs of lines. Each pair of lines corresponds to a transition to one of the vibrational levels of the X state, whereas the pair is a result of the rotational selection rule which allows $\Delta J = \pm 1$. The intensities of these lines are determined by the Franck-Condon factors.

For several years now, measurements of these resonance doublets have been used to calculate the spectroscopic constants for the ground state. The most recent and widely accepted results obtained by D. H. Rank and B. S. Rao[26] are listed in Table I.

The spectroscopic constants for the $B^3\pi_{ou}^+$ state have proven more difficult to measure. Even the assignment of vibrational quantum numbers for absorption bands, which was customarily accepted for

TABLE I.

Spectroscopic Constants for the Ground State of Molecular Iodine
(Rank and Rao[26])

$$T_e = 0$$

$$\omega_e = 214.51886$$

$$\omega_e x_e = 0.60738$$

$$\omega_e y_e = 1.307 \times 10^{-3}$$

$$\omega_e z_e = -5.04 \times 10^{-6}$$

$$B_e = 0.037289$$

$$\alpha_e = 0.001210$$

$$\beta_e = 1.9 \times 10^{-8}$$

$$\gamma_e = 8.57 \times 10^{-11}$$

$$D_e = -4.54 \times 10^{-9}$$

$$\beta_e^r = 1.20 \times 10^{-11}$$

nearly thirty years, has recently been revised. The latest measurements by Steinfeld, et al,[27] are listed in Table II.

C. Thermal Population of the I_2 Ground State

Inasmuch as iodine normally exists as a solid at room temperature, and all of the effects we are interested in occur in iodine vapor, it is necessary to examine its vapor characteristics. Most handbooks of chemistry and physics have tables which show how the vapor pressure depends on temperature, and also what the melting and boil points are. Figure 3 is a graph of this information.[28]

It is easily seen that small increases in temperature increase the vapor pressure very rapidly. This provides a simple method of controlling the density of the I_2 vapor, but it also introduces an additional problem. The population of the vibrational and rotational levels of the ground state is temperature dependent. The population of the vibrational levels follows a normal (Boltzmann) distribution with the number of molecules in any level, n, given by

$$N_n = \frac{N}{Q_\upsilon} e^{-\frac{E}{kT}} \tag{127}$$

where N is the total number of molecules and the parition function is

$$Q_\upsilon = 1 + e^{-\frac{E_1}{kT}} + \ldots = \sum_n e^{-\frac{E_n}{kT}} \tag{128}$$

TABLE II.

Spectroscopic Constant for the $B^2\pi_{ou}^+$ State of Molecular Iodine
(Steinfeld, et al[27])

$$T_e = 15770.59$$

$$\omega_e = 125.273$$

$$\omega_e x_e = 0.7016$$

$$\omega_e y_e = - 0.00567$$

$$\omega_e z_e = 0.000032$$

$$B_e = 0.028969$$

$$\alpha_e = 0.001562$$

$$\beta_e = - 4.0 \times 10^{-7}$$

$$\gamma_e = - 3.5 \times 10^{-8}$$

$$D_e = 3.5 \times 10^{-9}$$

$$\beta_e = 3.9 \times 10^{-10}$$

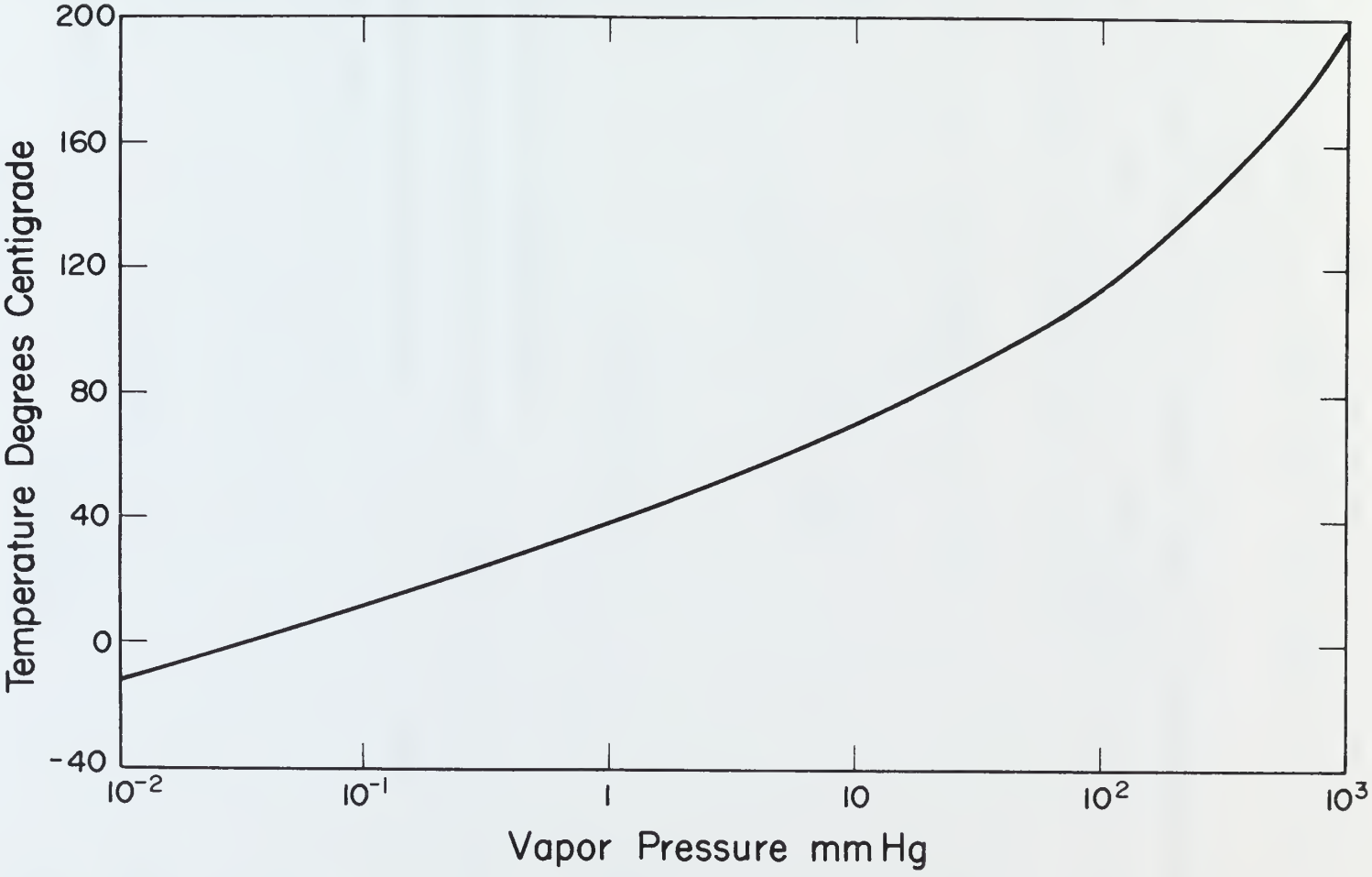

FIGURE 3. Iodine Vapor Pressure

using $E_o = 0$. What this means for the case of I_2 is that at room temperature nearly 23% of the molecules are in the first excited vibrational level and at 1000^oK nearly 74% as many are in it as are in the ground state.

The population of the rotational levels is a different matter. Each of the levels, J, have a 2J + 1 fold degeneracy, which means that the number, N_J, in this level is given by

$$N_J = \frac{(2J + 1)}{Q_r} N_n e^{-\frac{E_J}{kT}} \tag{129}$$

where

$$Q_r = \sum_J (2J + 1) e^{-\frac{E_J}{kT}} \tag{130}$$

and

$$E_J = hcB_U J(J + 1) \tag{131}$$

F(J) is given by equation (126).

In most instances, the model of a rigid rotator is a good approximation and the coefficient of $J^2(J + 1)^2$ is so small that it can be neglected. In this case

$$F(J) = B_U J(J + 1) \tag{132}$$

and

$$E_J = hcB_U H(J + 1) \tag{133}$$

This gives

$$Q_r = \sum_J (2J + 1) e^{-\frac{J(J + 1)hcB_U}{kT}} \tag{134}$$

which, for large T or small B_v, can be approximated by

$$Q_r = \int_0 (2J + 1)\, e^{-\frac{J(J+1)hcB}{kT}}\, dJ = \frac{kT}{hcB} \tag{135}$$

The result is that

$$N_J = N_n \frac{hcB}{kT}(2J + 1)\, e^{-\frac{J(J+1)hcB}{kT}} \tag{136}$$

By setting $\frac{dN_J}{dJ} = 0$, we find that N has a maximum when

$$J_{max} = \left(\frac{kT}{2B\ hc}\right)^{\frac{1}{2}} - \frac{1}{2} \tag{137}$$

For iodine at room temperature

$$J_{max} = 61 \tag{138}$$

The distribution over the rotational levels is the same for each vibrational level with only the total number of each vibrational level, N_n, being different.

V. NEODYMIUM-DOPED GLASS

A. Energy Levels

Neodymium and other rare-earths have the most complicated spectra of any of the elements. This is due to the incomplete 4f shell which produces a large number of low-lying energy levels. The absorption and fluorescence spectra of triply ionized neodymium ion (Nd^{3+}) in crystals has been studied extensively. Term assignments have been made by Carlson and Dieke.[29] The studies were generally made in a variety of host crystals; consequently, there are differences in level positions within a given multiplet, depending on the host lattice. Since the energy levels of rare-earth ions in solids are highly shielded by the outer electronic shells, the energy levels are very similar to those of the free ion.[30]

Figure 4 shows the energy levels of neodymium as given by Dieke and Crosswhite,[31] and also the energy levels of Nd^{3+} in $CaWO_4$ as given by Johnson.[32] In the case of Nd-doped glass, the levels are essentially the same. There are several transitions which may produce laser action, but the most commonly used and most efficient is the ${}^4F_{\frac{3}{2}} \rightarrow {}^4I_{\frac{11}{2}}$ transition at a wavelength of 1.06μ.

B. Absorption Spectrum

The absorption spectrum of Nd^{3+} in glass is given in Figure 5.[33]

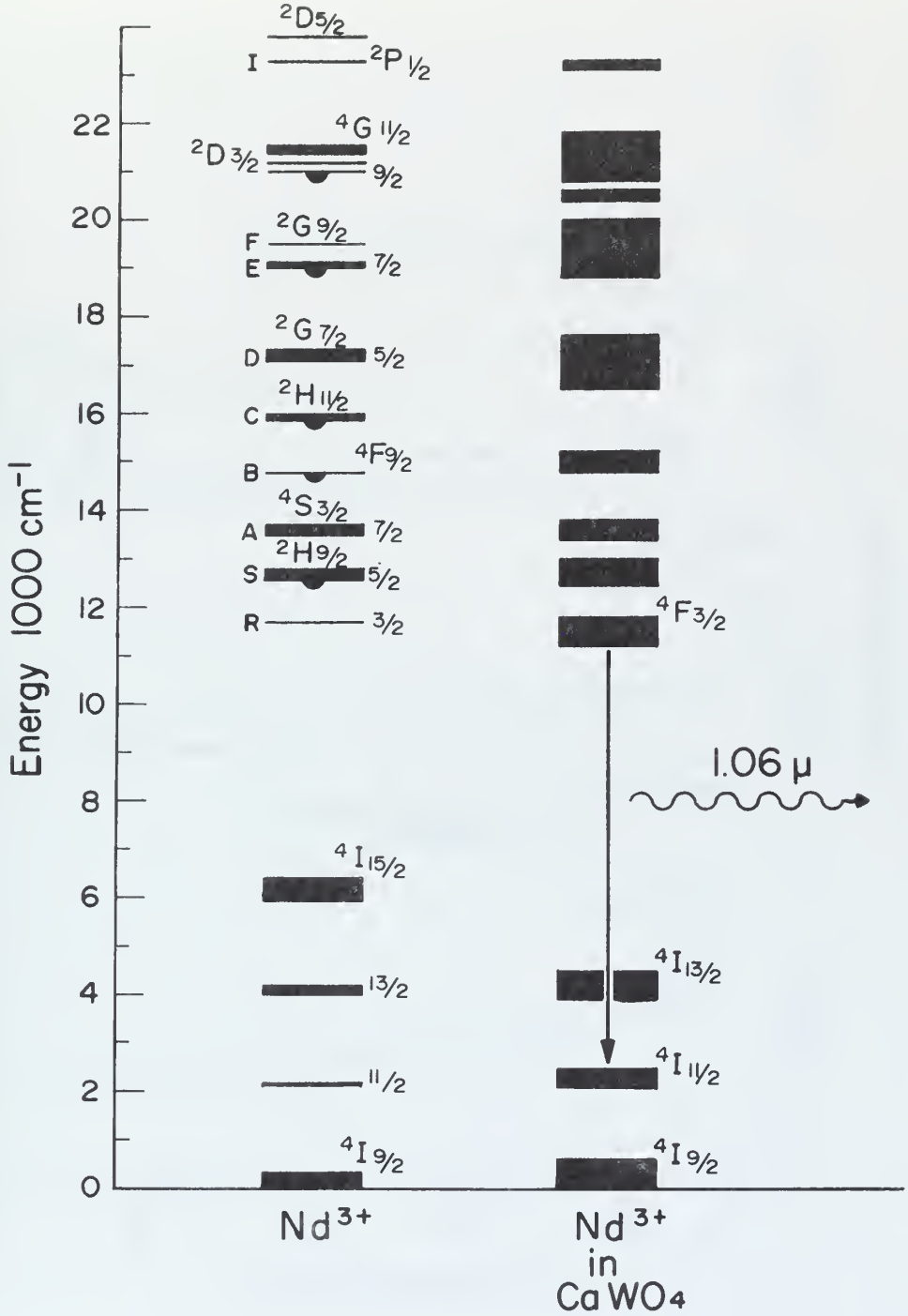

FIGURE 4. Energy Levels of Neodymium
(after Dieke and Crosswhite[31] and Johnson[32])

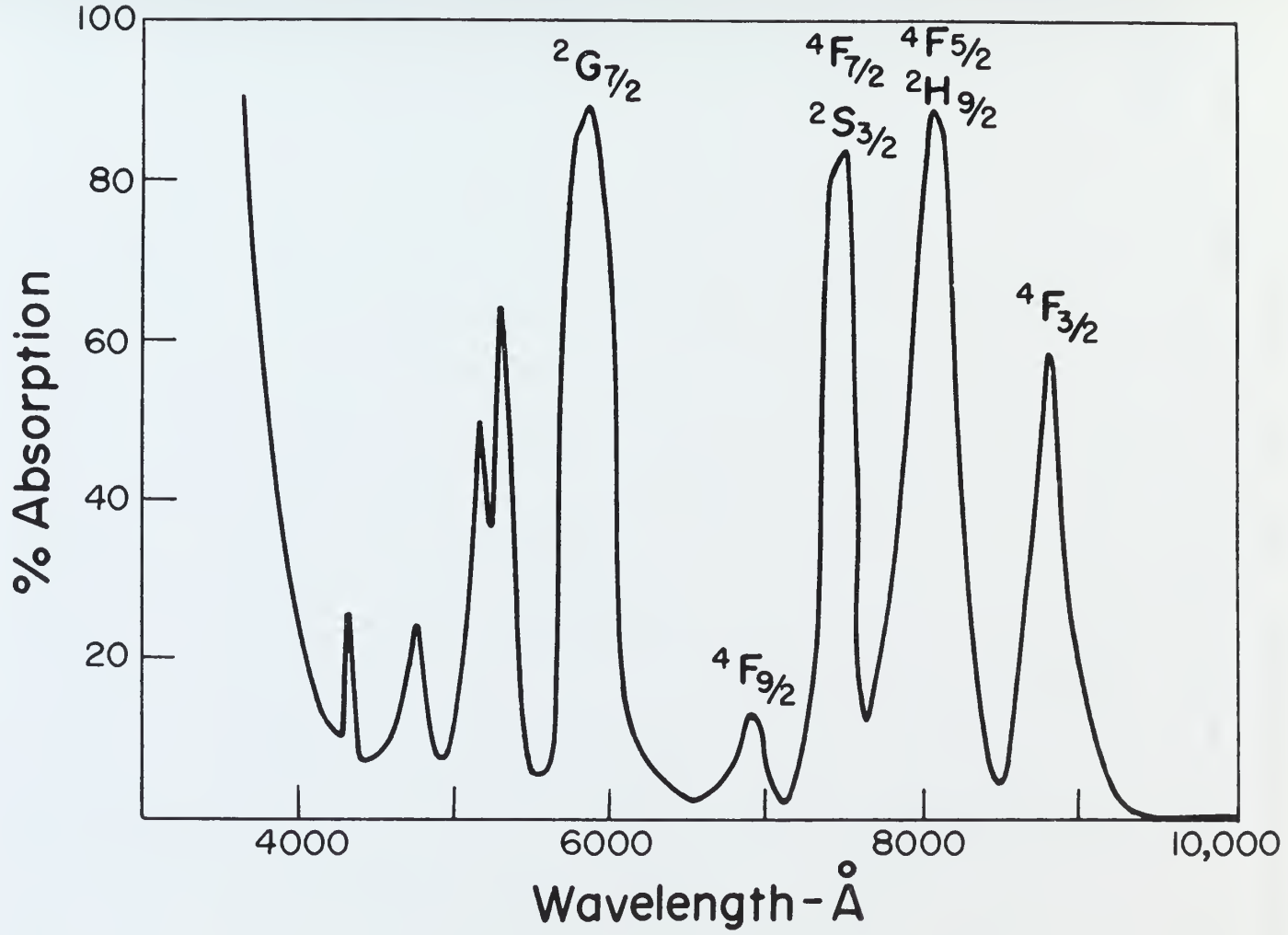

FIGURE 5. Absorption Spectrum of Nd^{3+} in Glass

Included as part of the figure are the probable transitions which give rise to each of the absorption bands. Ions excited to any of the higher levels will decay with a very high quantum efficiency into the $^4F_{\frac{3}{2}}$ level which has a very long lifetime (τ_{spe} ~ 1 millisecond).

VI. EXPERIMENTAL

A. Aims of the Experiment

This research was originally designed to consist of two parts. The first part was concerned with the absorption of Q-switched laser light in iodine. In chapter IV of this paper, we discussed the energy levels of iodine and mentioned its strong fluorescence. In the introduction, we also mentioned that Sorokin and Lankard[3] had observed stimulated fluorescence in organic dyes. Since the fluorescence in iodine was strong, it was felt that perhaps the iodine would undergo stimulated fluorescence if excited by strong light in the green part of the spectrum. For this reason, a study of the absorption spectrum near 5300Å in iodine was undertaken. A frequency-doubling crystal of ADP was added to the K - 1 Q Nd laser to convert part of the 1.06μ light to 5300Å. The output beam was then passed through iodine and the spectrum was analysed to detect any effects which may have occurred in the iodine. As an extension of this part, the beam from the ruby laser at 6943Å was also passed through iodine vapor at various temperatures and pressures in order to examine any effects produced.

The second part of the research was motivated by the reports of Briquet, Jego, and Terneaud,[9] and Ross and Zeidler.[34] These papers both reported pulses of stimulated emission at 1.06μ when Nd-doped

glass was pumped by intense laser light. Eckhardt and Hellwarth, et al,[3] had reported stimulated Raman emission in benzene with a shift of 991 cm^{-1}. This means that it would be possible to obtain intense pulses of light at 7458Å, 8053Å, and 8751Å by passing the beam from a ruby laser through benzene. The three wavelengths correspond to the first, second, and third order Stokes lines respectively. These Stokes lines occur at wavelengths coincident with strong absorption bands in Nd-doped glass as shown in Figure 5. The aim of the second part of the research, therefore, was to examine the possibility of optically pumping Nd-doped glass with light from the stimulated Stokes Raman lines of benzene and thereby producing stimulated emission at 1.06μ.

During the investigation of the light interactions in the Nd-doped glass, it was discovered that stimulated light was being emitted over a broad frequency band of the spectrum. This light did not originate in the Nd-doped glass. Thus, a further aim of the research was to trace the source and nature of this broad-band emission.

B. Description of the Experimental Apparatus

1. K - 1 Q Pockels Laser System

The K - 1 Q laser system was manufactured by the Korad Division of the Union Carbide Company. The laser produces intense light pulses in the 10 to 100 Megawatt range, using either a neodymium-doped glass

rod or a ruby rod as the oscillator medium.

A block diagram of the system is given as Figure 6. The output mirror is a 3.3mm thick sapphire resonant reflector. The laser head contains either the ruby or Nd rod, surrounded by a spiral Xenon flash lamp, and a ceramic reflector, all mounted within the head container. The head container is filled with circulating distilled water for cooling purposes. When the Nd rod is used, a polarizer must be installed in the system between the laser rod and the pockels cell to selectively pass light of the proper (horizontal) polarization. This is not necessary when using the ruby laser, because the ruby rod is cut with its axis parallel to the "c" plane of the crystal and therefore can be oriented to selectively pass light of the proper (horizontal) polarization.

A pockels-cell light shutter, located between the horizontal and vertical polarizers, is used when operating the laser system in the Q-switched mode. Since crossed polarizers are located between the reflectors of the laser cavity, the only way to have a low loss for the passage of light through the cavity is to rotate the polarization of light by 90^{o} as it passes through the pockels cell. This can be done by applying the proper voltage to the pockels crystal.

When the flash lamp fires, the population of the $^{4}F_{\frac{3}{2}}$ level in the neodymium rod or the $^{2}E(\overline{E})$ level in the ruby rod increases to a maximum value in a few hundred microseconds. If the proper voltage

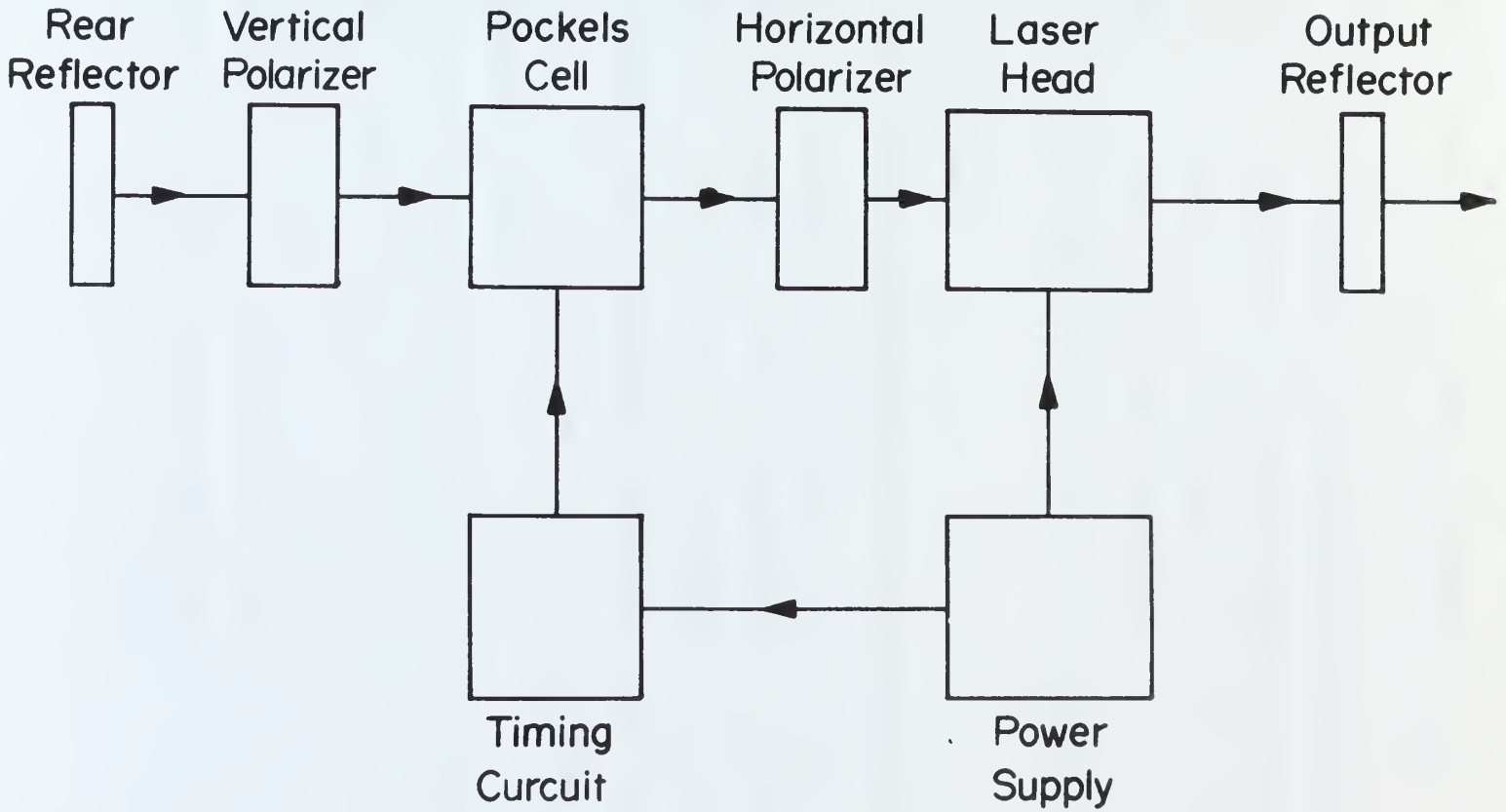

FIGURE 6. Korad K - 1 Q Laser System

is timed to be applied across the pockels cell within a few microseconds of when this maximum population inversion occurs, then the output of the laser will consist of a giant pulse of a few nanoseconds duration.

The rear reflector is interchangeable for either the ruby or Nd rod. The reflectors are multilayer dielectric mirrors coated for 100% reflectivity at 6943Å in the case of ruby or 100% reflectivity at 10,600Å in the case of neodymium.

The rated output of the system is given in Table III.

2. Spectrographs

Two different spectrographs were used in this experiment. Both were of local design and manufacture. The first one had low dispersion and was used for searching large portions of the spectrum. It consisted of a flat ruled grating of 15,000 lines per inch mounted in a Zerney-Turner arrangement. The mirrors had a focal length of 50 cm. The first order dispersion of the spectrograph was 31Å per millimeter at 7000Å.

The second spectrograph was used for high resolution. It contained a Bausch and Lomb echelle grating mounted in a two lens "V" arrangement using two 1-meter achromatic lenses. The grating had 73.25 lines per millimeter blazed at an angle of 63° 26'. This resulted in the highest efficiency when operated in the 44th or 45th order near 5300Å and the 34th order of 6943Å. In the 45th order,

TABLE III

Rated Output of the K-1Q Laser System

	Ruby	Neodymium
Wavelength	6943 A	10,600 A
Line width per spectral element	0.1 A	0.4 A
Peak power	50 megawatts	70 megawatts
Pulse energy	1.0 joules	2.0 joules
Pulse width	10-20 nanoseconds	15-25 nanoseconds
Beam size (diameter)	3/8 inch	1/2 inch

the dispersion was 1Å per millimeter, and in the 34th order it was 1.4Å per millimeter.

3. Photomultipliers.

Two photomultipliers were used for detection of light in these experiments. An RCA 1P21 was used to minotor the output of the K - 1 Q ruby laser. This tube has a minimum rise time of 2 nanoseconds, but the shunt capacitance and coupling resistance used in the associated circuitry establish the rise time of the system at 100 nanoseconds. The tube has an S-4 spectral response as shown in Figure 7.

An RCA 7102 was used to detect the frequency-shifted light. This tube has a rise time of a few nanoseconds. With the circuitry used in this experiment, it was possible to obtain a rise time for the system of 10 nanoseconds. The tube has an S-1 spectral response as also shown in Figure 7.[35]

4. Optical Attenuators.

The high power density of the output from Q-switched lasers is very difficult to handle. It destroys interference filters, vaporizes the coatings from mirrors, chars the bonding material in achromatic lenses, etches the surfaces of spectrograph slits, and it can even pit or pulverize glass in the optical systems if handled incorrectly. The excessive power of the laser beam, even

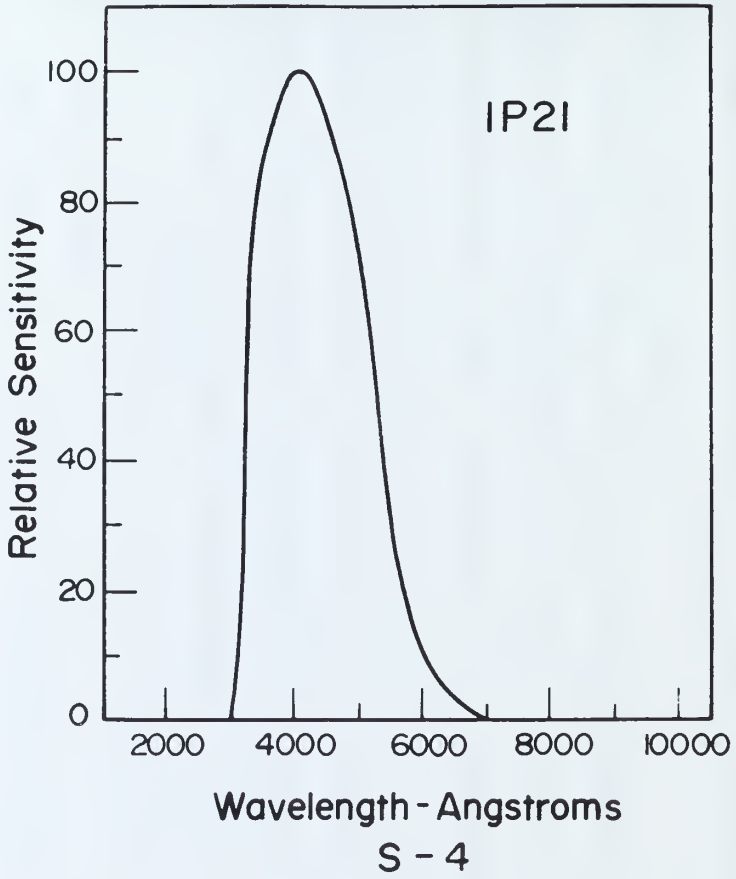

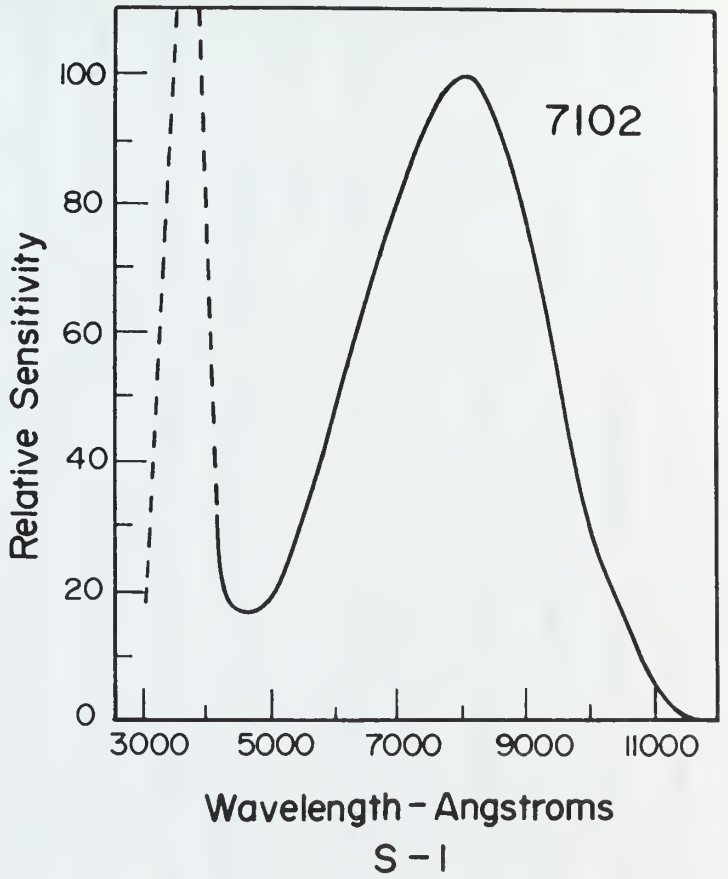

FIGURE 7. S-1 and S-4 Spectral Response Curves

after it had passed through the material in which the interaction was being studied, was somewhat of a nuisance and required attenuation for most of the experiments. Sorokin, Shirer, et al,[36] reported using a solution of $CuSO_4$ in water as an optical attenuator. This was tried by the author, but it was found that the attenuation was greater in the spectral region where interactions were to be examined (7000Å - 1.2μ) than it was at the wavelength of the laser output (6943Å).

Brode[37] discussed the absorption of cobalt halides in their respective halogen acid and this absorption appeared to be in the proper spectral regions. A 5 cm long cell and a 10 cm long cell containing $CoCl_2$ in HCl were prepared and used in this experiment. A 5 cm long cell containing $CoBr_2$ in HBr was also used. Spectrophotometer traces of the absorption of each of these attenuating cells are shown in Figure 8.

The $CoCl_2$ in HCl is an ideal filter for removing light at 6943Å while passing essentially all light of wavelength greater than 7200Å but less than 1.1 microns. To the best knowledge of the author, he is the first to use this material for this purpose. The experiment involving the interaction of stimulated Raman-shifted light in neodymium-doped glass was considered feasible only because the $CoCl_2$ in HCl attenuator was available.

5. Iodine System.

The iodine system consisted of an evacuated glass cell which

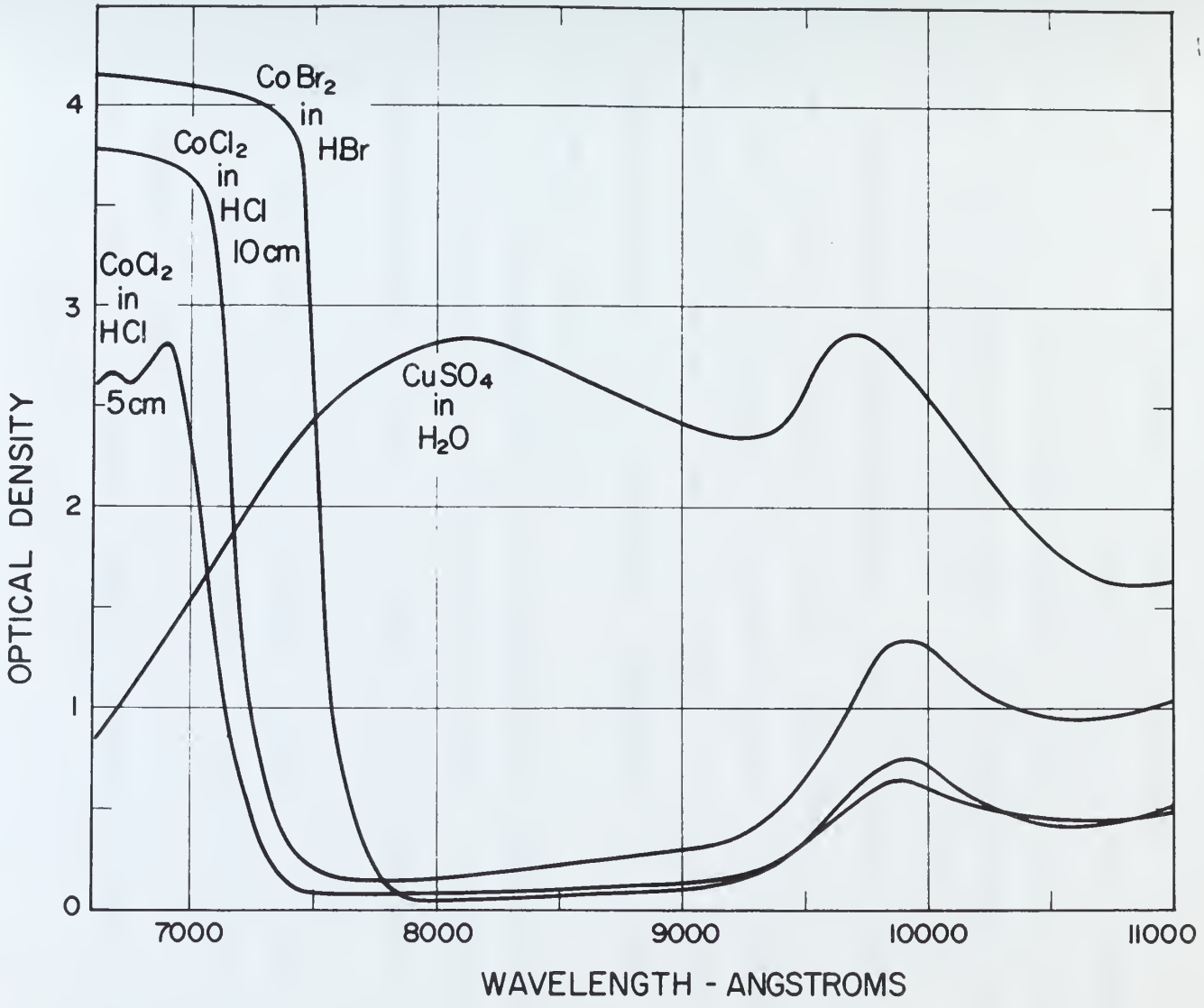

FIGURE 8. Absorption Spectra of $CuSO_4$, $CoCL_2$ in HCl, $CoBr_2$ in HBr Optical Attenuating Cells

contained iodine crystals. Ground glass filters or optical attenuating cells were used to attenuate the beam after it had passed through the iodine. Three different iodine cells were used. The first was 1 meter in length and 24 mm in internal diameter. It was fitted with Brewster windows of commercial manufacture on both ends. The second was a shorter (30 cm) version of the first and the third was a 20 cm cell with an inside diameter of 28 mm. This latter cell was of local manufacture and the windows were made from flat pyrex glass. The windows were approximately normal to the light path.

The first two iodine cells were wrapped with electric heating tape. They could be maintained at uniform temperatures up to 75°C. The third (short) was heated by using metal jackets. These jackets extended beyond the end windows and prevented the windows from cooling by convection of air or radiation. Temperatures up to 150°C were possible using this cell.

All of the measurements for the interaction of light in iodine were taken using the high dispersion spectrograph. The system was arranged as shown in Figure 9. The beam splitter located between the laser and the iodine cell was used to divert a small part (< 10%) of the light directly to the spectrograph, bypassing the iodine cell. This portion of the light was focused onto the lower portion of the spectrograph slit and was attenuated by a ground glass plate. This light was used as a reference to indicate the spectral composition of the direct output of the laser.

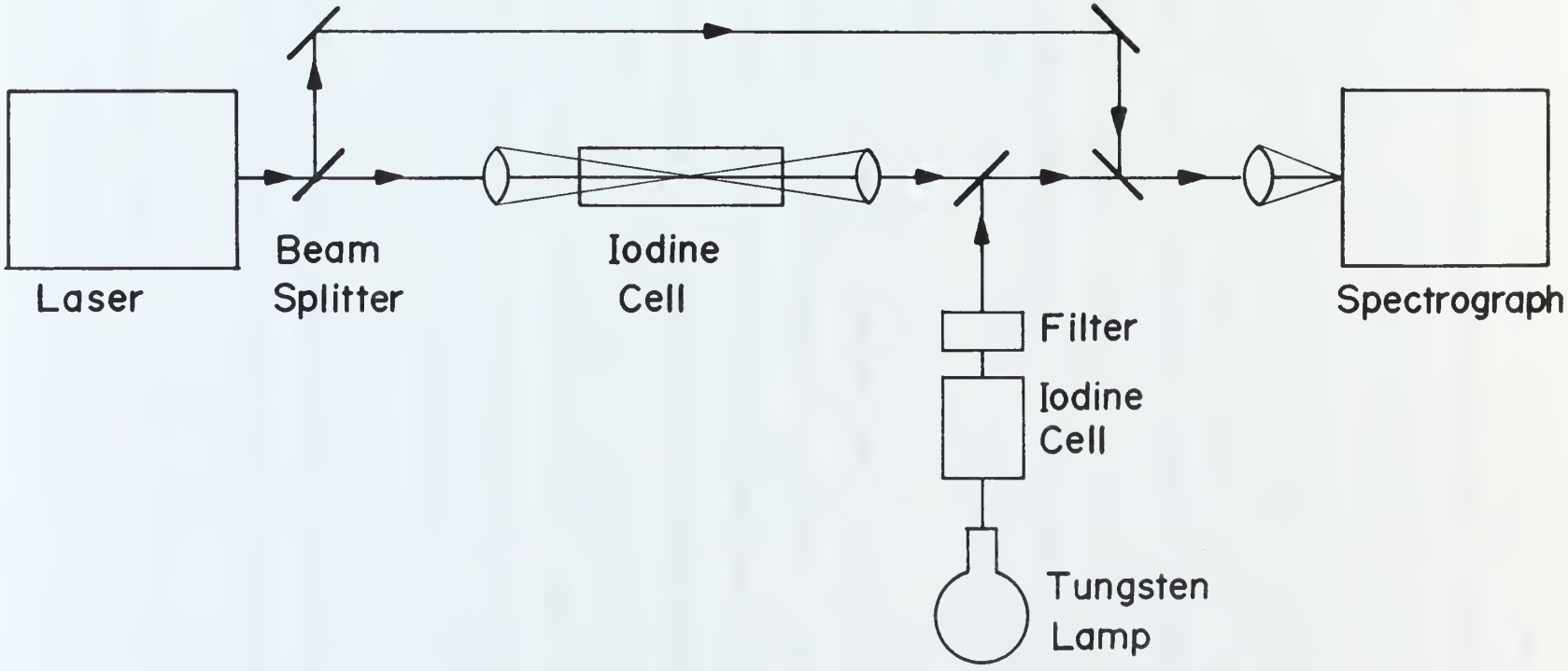

FIGURE 9. Spectrograph Detection with the Iodine System

The major part of the output from the laser passed directly through the iodine cell and was then focused onto the central portion of the slit. It was also attenuated by passing it through a ground glass plate.

For an additional reference, light from a tungsten source was passed through iodine vapor and focused on the top portion of the spectrograph slit. An interference filter or monochromator was used between the iodine and the slit to assure that light from only one order passed through the spectrograph. A neon spectrum was superimposed on the absorption spectrum to provide wavelength calibration.

Various photographic films were used for detection by spectrograph, depending on the wavelength of interest. For the visible region near 5300Å, polaroid type 107 film was used for preliminary investigations and Kodak TRI-X was used for taking final spectrographic data. Polaroid type 413 was used for preliminary investigations near 6943Å and in the near infrared up to 9000Å. Kodak plates with type I-N emulsion were used for final measurements in this same region. Figure 10 shows the spectral sensitivities of each type emulsion or film.[38,39]

Measurements of wavelength were made with either a traveling microscope or taken from the tracing of a photodensitometer.

6. Neodymium-Glass System.

This system consisted of a benzene cell, a filter cell, a

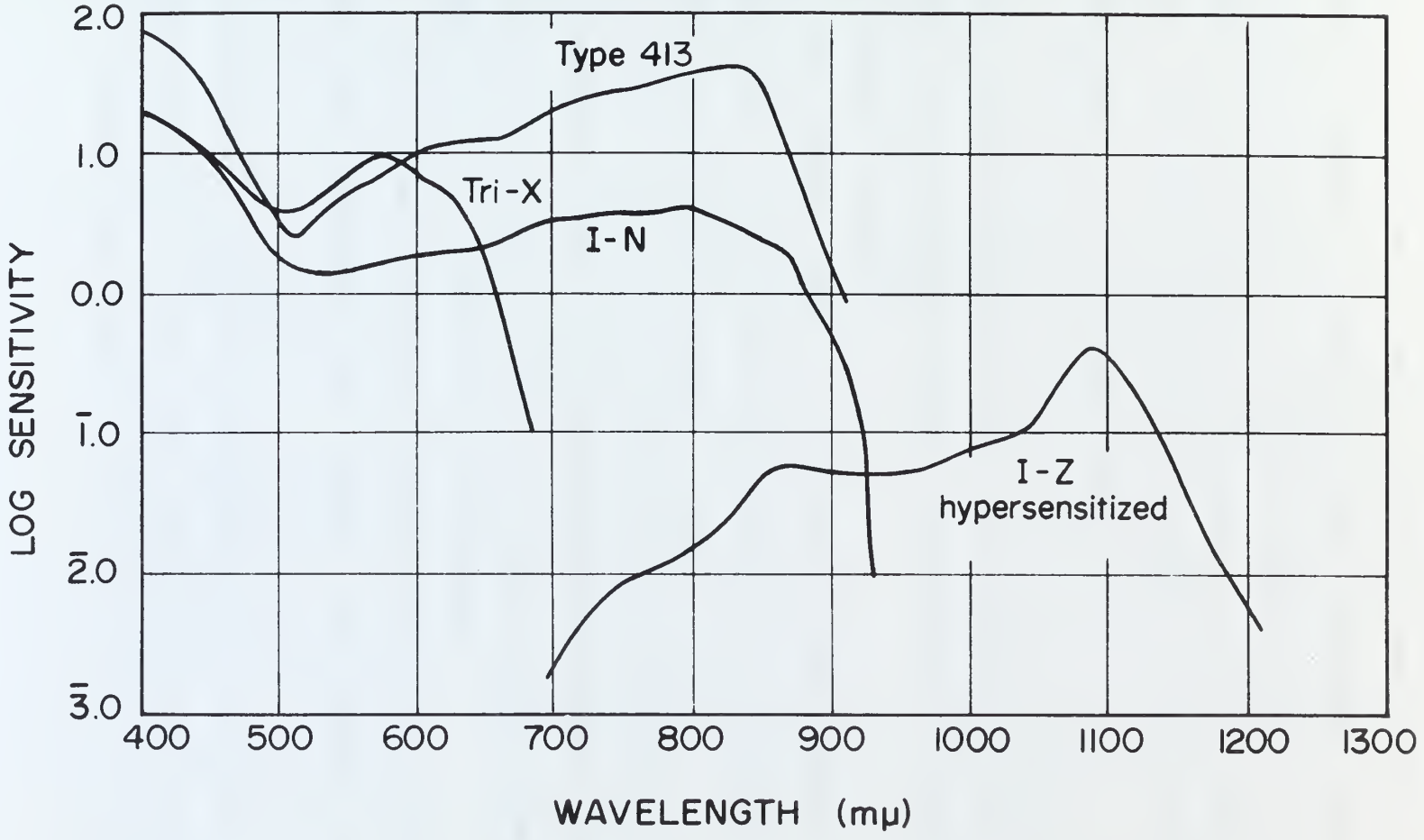

FIGURE 10. Spectral Sensitivities of Photographic Detectors

neodymium glass rod, and mirrors to form an optical cavity. The benzene cell was used to produce stimulated Raman radiation at the first, second, and third order Stokes frequencies as previously mentioned. The cell was a cylindrical pyrex container 30 cm in length, filled with reagent grade benzene. It had an inside diameter of 28 mm and the end windows were made of flat pyrex glass. The container was of local manufacture.

The filter cells in the system were 5 and 10 cm in length and constructed in the same manner as the benzene cell. They were filled with various solutions as discussed in the section on optical attenuators.

The neodymium glass rod is the same rod used in the K - 1 Q laser system. It is 6 inches long and ½ an inch in diameter. The absorption spectrum of the glass is given in Figure 5.

The mirrors used to form the cavity had reflectances as given by the curves in Figure 11. Two mirrors matching each of the reflectance curves were available so the cavity could be formed by using a variety of combinations of the mirrors.

Light interactions in the neodymium glass system were detected using the photomultiplier system. The arrangement is shown in Figure 12. The photomultipliers were connected to the two inputs of a Tektronix 565 dual beam oscilloscope, except for pulse width measurements which were made with a Tektronix 519 oscilloscope. The oscilloscope was triggered with the pulse from the Pockels-cell

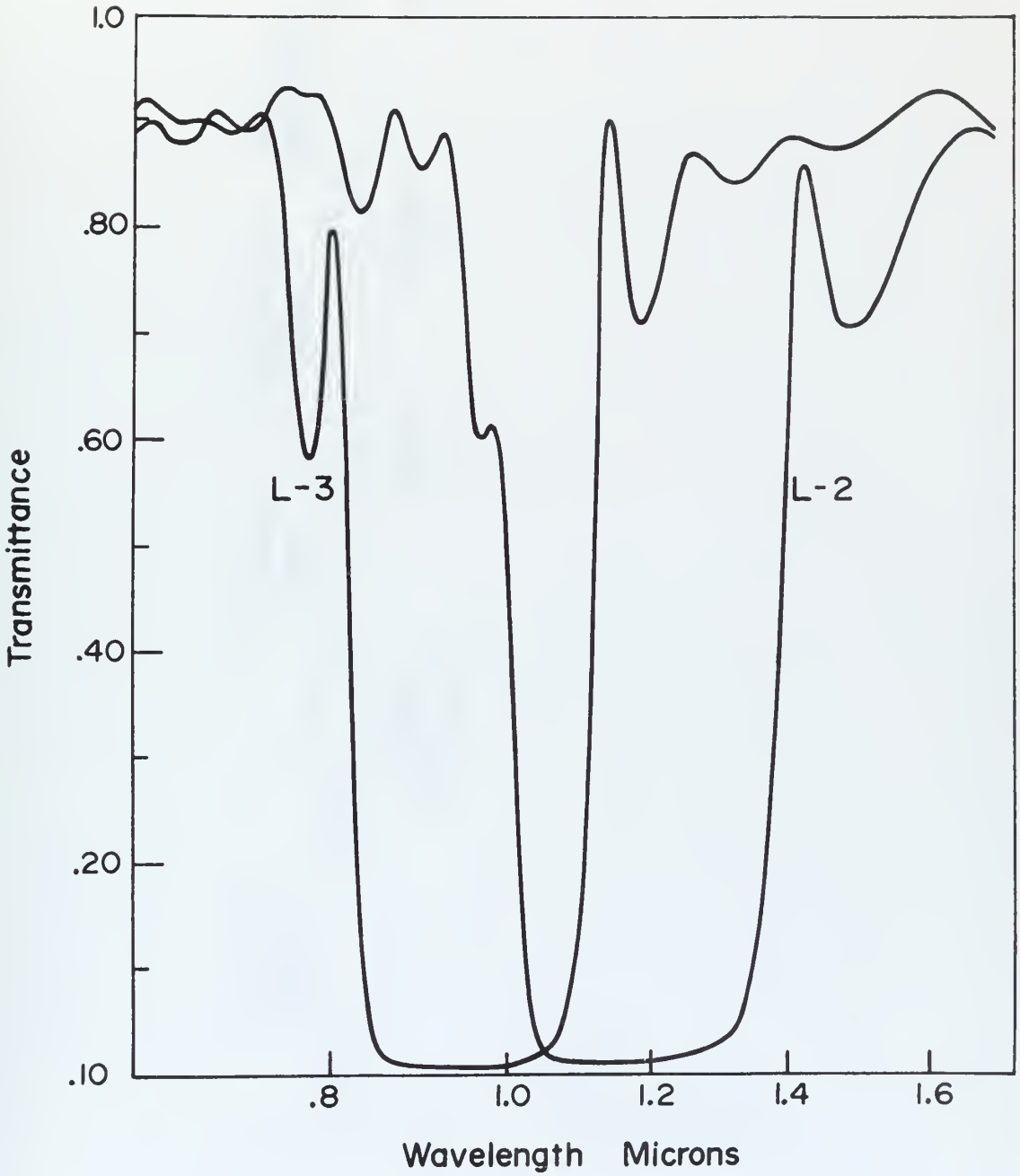

FIGURE 11. Reflectance Curves of Dielectric Mirrors

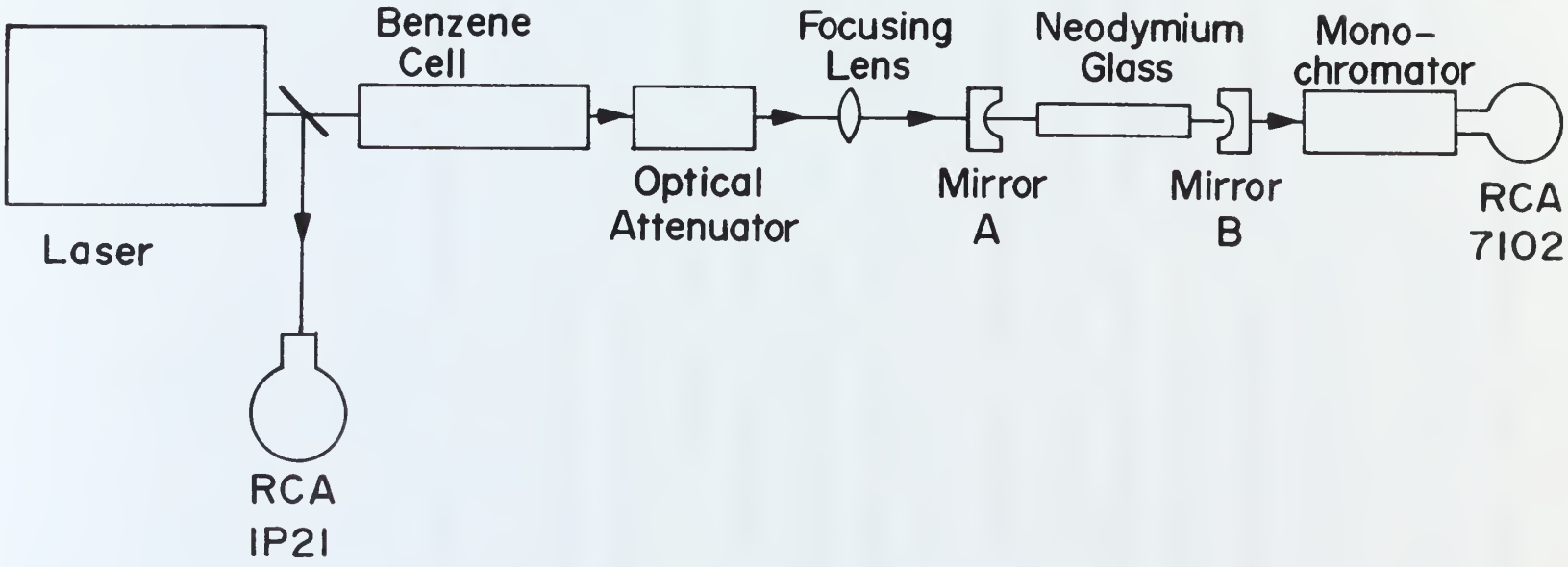

FIGURE 12. Photomultiplier Detection with Neodymium-Doped Glass System

trigger in the K - 1 Q laser system. This provided a delay of approximately 0.8 microseconds from the start of the sweep until the light pulse reached the photomultipliers. The Tektronix 519 was triggered internally or triggered with the output of the monitor RCA 1P21 photomultiplier.

The monochromator used in conjunction with the RCA 7102 photomultiplier was a small grating instrument made by Bausch and Lomb. The intensity of the light pulse entering the monochromator was occasionally so great that it reached the photomultiplier by reflecting from the black walls of the monochromator, even with the slit set at less than 50 microns width. This gave a pulse on the oscilloscope regardless of where the monochromator dial was set. To prevent this happening, a piece of ground glass plate was inserted in front of the slit. With the ground glass in place, and the slit width set at 250 microns, the monochromator had a resolution of approximately ± 50Å at half intensity.

The spectral composition of the light in the neodymium system was determined with the low dispersion spectrograph. Kodak plates with type I-Z emulsion were used in this system. The emulsion is sensitive to light at wavelengths up to 1.2 microns. A spectral sensitivity curve is included in Figure 10.

VI. RESULTS AND CONCLUSIONS

A. Iodine

The first part of the experiment with iodine consisted of a spectroscopic analysis of the absorption spectrum of iodine near 5310Å and near 6943Å using a tungsten lamp source with appropriate filters. The wavelengths in air of the absorption lines were calculated using the constants of Rank and Rao[26] (Table I), and Steinfeld, et al,[27] (Table II). The lines calculated for 5300Å to 5320Å are listed in Table IV. Only the bands involving transitions from the ground, first excited, or second excited vibrational levels of the ground electronic state are considered. These are the only levels which contain an appreciable number of molecules at the operating temperature. Table V contains the listing of lines calculated in the region of 6930Å to 6950Å. The calculations indicate that band heads exist at 5307.74Å and 6931.99Å.

Wavelength measurements of the absorption lines of iodine in the region of 5300Å to 5320Å are listed in Table VI. These measurements were taken from photodensitometer traces of the TRI-X film used to record the spectrum. A neon spectrum was superimposed on the absorption spectrum and used as a wavelength reference. Measurements from the photodensitometer trace were converted to wavelength by means of a second degree polynomial. This polynomial was

obtained by using a least squares method to fit measurements of the neon spectrum to the known wavelengths. Not all neon lines were used in the least squares method. Those which were not used to obtain the polynomial were used to check its accuracy. Errors obtained when calculating the wavelengths of these additional neon lines were ± 0.02Å.

Wavelengths were measured from three separate plates and the average listed in Table VI. The measured wavelengths from each plate differed at most by 0.03Å from either of the other plates. The maximum standard deviation is, therefore, 0.013Å. Lines of equal intensity were resolved only if they were separated by 0.04Å or more.

Measurements of the absorption lines from 6930Å to 6950Å were made using the same method as was employed to measure the lines near 5310Å. The spectrum was recorded on Kodak Type I-N plates. The maximum standard deviation was 0.07 Å and lines of equal intensity were resolved only if separated by 0.07 Å or more. Table VII contains the listing of these lines.

The measured spectrum was not sufficiently resolved to allow a line-by-line comparison with the calculations. The presence of band heads at a measured wavelength of 5308.03Å and 6936.2Å can be compared directly with the calculated band heads at 5307.74Å and 6931.99Å.

TABLE IV

CALCULATED ABSORPTION LINES IN IODINE VAPOR,
5300Å TO 5320Å

λ air (Å)	υ''	υ'	J''	J'	λ air (Å)	υ''	υ'	J''	J'
5300.01	0	34	81	82	5301.44	0	34	83	84
5300.02	0	36	117	118	5301.49	1	36	28	29
5300.09	1	36	19	18	5301.53	0	35	103	104
5300.10	1	38	83	82	5301.54	0	33	51	50
5300.17	1	36	22	23	5301.60	0	33	54	55
5300.20	1	37	63	64	5301.64	1	36	26	25
5300.21	0	33	48	47	5301.68	1	37	63	62
5300.27	0	33	51	52	5301.68	1	38	85	84
5300.29	1	36	20	19	5301.72	0	36	116	115
5300.32	0	35	99	98	5301.74	1	36	29	30
5300.37	1	36	23	24	5301.90	1	36	27	26
5300.49	1	36	21	20	5301.98	1	37	66	67
5300.50	1	37	61	60	5302.00	0	33	52	51
5300.51	1	38	86	87	5302.00	0	34	81	80
5300.56	0	34	79	78	5302.00	1	36	30	31
5300.57	1	36	24	25	5302.07	0	33	55	56
5300.64	0	33	49	48	5302.10	1	38	88	89
5300.65	0	36	115	114	5302.15	0	35	101	100
5300.70	0	33	51	52	5302.16	1	36	28	27
5300.70	1	36	22	21	5302.17	0	34	84	85
5300.72	0	34	82	83	5302.18	0	36	119	120
5300.79	1	36	25	26	5302.27	1	36	31	32
5300.79	1	37	64	65	5302.29	1	37	64	63
5300.88	1	38	84	83	5302.44	1	36	29	28
5300.92	1	36	23	22	5302.45	0	35	104	105
5301.01	1	36	23	27	5302.47	0	33	53	52
5301.09	0	33	50	49	5302.49	1	38	86	85
5301.09	1	37	62	61	5302.54	0	33	56	57
5301.10	0	36	118	119	5302.55	1	36	32	33
5301.15	0	33	53	54	5302.59	1	37	67	68
5301.15	1	36	24	23	5302.72	1	36	30	29
5301.23	0	35	100	99	5302.73	0	34	82	81
5301.25	1	36	27	28	5302.81	0	36	117	116
5301.27	0	34	80	79	5302.84	1	36	33	34
5301.30	1	38	87	88	5302.90	1	37	65	64
5301.38	1	37	65	66	5302.91	0	34	85	86
5301.39	1	36	25	24	5302.92	1	38	89	90

TABLE IV--Continued

λ air (Å)	υ''	υ'	J''	J'	λ air (Å)	υ''	υ'	J''	J'
5302.95	0	33	54	53	5304.81	1	37	68	67
5303.02	0	33	57	58	5304.95	0	33	58	57
5303.02	1	36	31	30	5304.96	0	35	104	103
5303.08	0	35	102	101	5304.96	1	38	89	88
5303.14	1	36	34	35	5304.97	1	36	37	36
5303.21	1	37	68	69	5304.99	0	34	85	84
5303.26	0	36	120	121	5305.00	0	36	119	118
5303.30	1	38	87	86	5305.02	0	33	61	62
5303.32	1	36	32	31	5305.11	1	36	40	41
5303.38	0	35	105	106	5305.12	1	37	71	72
5303.44	0	33	55	54	5305.17	0	34	88	89
5303.44	1	36	35	36	5305.28	0	35	107	108
5303.48	0	34	83	82	5305.33	1	36	38	37
5303.51	0	33	58	59	5305.41	1	38	92	93
5303.53	1	37	66	65	5305.46	1	37	69	68
5303.63	1	36	33	32	5305.47	0	36	122	123
5303.65	0	34	86	87	5305.48	0	33	59	58
5303.74	1	38	90	91	5305.48	1	36	41	42
5303.76	1	36	36	37	5305.55	0	33	72	63
5303.84	1	37	69	70	5305.70	1	36	39	38
5303.90	0	36	118	117	5305.76	0	34	86	85
5303.93	0	33	56	55	5305.78	1	37	72	73
5303.95	1	36	34	33	5305.80	1	38	90	89
5304.00	0	33	59	60	5305.85	1	36	42	43
5304.02	0	35	103	102	5305.92	0	35	105	104
5304.08	1	36	37	38	5305.94	0	34	89	90
5304.13	1	38	88	87	5306.01	0	33	60	59
5304.16	1	36	67	66	5306.07	1	36	40	39
5304.23	0	34	84	83	5306.08	0	33	63	64
5304.28	1	36	35	34	5306.12	0	36	120	119
5304.33	0	35	106	107	5306.12	1	37	70	69
5304.36	0	36	121	122	5306.23	1	36	43	44
5304.41	0	34	87	88	5306.24	0	35	108	109
5304.42	1	36	38	39	5306.25	1	38	93	94
5304.33	0	33	57	56	5306.45	1	37	73	74
5304.48	1	37	70	71	5306.46	1	36	41	40
5304.51	0	33	60	61	5306.54	0	34	87	86
5304.57	1	38	91	92	5306.55	0	33	61	60
5304.62	1	36	36	35	5306.59	0	36	123	124
5304.76	1	36	39	40	5306.62	0	33	64	65

TABLE IV--Continued

λ air (Å)	υ''	υ'	J''	J'	λ air (Å)	υ''	υ'	J''	J'
5306.62	1	36	44	45	5308.01	0	32	6	5
5306.66	1	38	91	90	5308.01	0	32	9	10
5306.73	0	34	90	91	5308.08	0	32	7	6
5306.79	1	37	71	70	5308.08	0	32	10	11
5306.85	1	36	42	41	5308.09	1	36	45	44
5306.89	0	35	106	105	5308.13	0	34	89	88
5307.01	1	36	45	46	5308.16	0	32	8	7
5307.10	0	33	62	61	5308.16	0	32	11	12
5307.11	1	38	94	95	5308.16	1	37	73	72
5307.13	1	37	75	75	5308.18	0	35	110	111
5307.17	0	33	65	66	5308.22	0	33	64	63
5307.20	0	35	109	110	5308.25	0	32	9	8
5307.24	0	36	121	120	5308.25	0	32	12	13
5307.26	1	36	43	42	5308.26	1	36	48	49
5307.33	0	34	88	87	5308.30	0	33	67	68
5307.42	1	36	46	47	5308.32	0	34	92	93
5307.47	1	37	72	71	5308.35	0	32	10	9
5307.52	0	34	91	92	5308.35	0	32	13	14
5307.52	1	38	92	91	5308.37	0	36	122	121
5307.65	0	33	63	62	5308.39	1	38	93	92
5307.67	1	36	44	43	5308.45	0	32	11	10
5307.71	0	36	124	125	5308.46	0	32	14	15
5307.73	0	33	66	67	5308.51	1	37	76	77
5307.74	0	32	0	1	5308.52	1	36	46	45
5307.74	0	32	1	2	5308.57	0	32	12	11
5307.74	0	32	2	3	5308.57	0	32	15	16
5307.75	0	32	3	4	5308.69	0	32	13	12
5307.77	0	32	1	0	5308.69	0	32	16	17
5307.78	0	32	4	5	5308.70	1	36	49	50
5307.80	0	32	2	1	5308.79	0	33	65	64
5307.81	0	32	5	6	5308.82	0	32	14	13
5307.81	1	37	75	76	5308.83	0	32	17	18
5307.84	0	32	3	2	5308.85	0	35	108	107
5307.84	0	32	6	7	5308.85	0	36	125	126
5307.84	1	36	47	48	5308.86	1	37	74	73
5307.86	0	35	107	106	5308.86	1	38	96	97
5307.89	0	32	4	3	5308.88	0	33	68	69
5307.89	0	32	7	8	5308.94	0	34	90	89
5307.94	0	32	5	4	5308.96	0	32	15	14
5307.95	0	32	8	9	5308.96	1	36	47	46
5307.98	1	38	95	96	5308.97	0	32	18	19

TABLE IV--Continued

λ air (Å)	υ"	υ'	J"	J'	λ air (Å)	υ"	υ'	J"	J'
5309.11	0	32	16	15	5310.53	1	36	53	54
5309.12	0	32	19	20	5310.57	0	33	68	67
5309.13	0	34	93	94	5310.58	0	34	92	91
5309.14	1	36	50	51	5310.60	0	32	24	23
5309.17	0	35	111	112	5310.61	0	32	27	28
5309.21	1	37	77	78	5310.64	1	38	98	99
5309.27	0	32	17	16	5310.65	1	37	79	80
5309.27	0	32	20	21	5310.66	0	33	71	72
5309.28	1	38	94	93	5310.67	0	36	124	125
5309.38	0	33	66	65	5310.77	0	34	95	96
5309.41	1	37	48	47	5310.82	1	36	51	50
5309.43	0	32	18	17	5310.83	0	32	25	24
5309.44	0	32	21	22	5310.84	0	32	28	29
5309.46	0	33	69	70	5310.84	0	35	110	109
5309.51	0	36	123	122	5311.01	1	36	54	55
5309.57	1	37	75	74	5311.02	1	37	77	76
5309.60	1	36	51	52	5311.06	0	32	26	25
5309.61	0	32	19	18	5311.07	0	32	29	30
5309.61	0	32	22	23	5311.07	1	38	96	95
5309.75	0	34	91	90	5311.15	0	36	127	128
5309.75	1	38	97	98	5311.17	0	35	113	114
5309.79	0	32	20	19	5311.18	0	33	69	68
5309.80	0	32	23	24	5311.27	0	33	72	73
5309.84	0	35	109	108	5311.30	0	32	27	26
5309.87	1	36	49	48	5311.30	1	36	52	51
5309.93	1	37	78	79	5311.31	0	32	30	31
5309.94	0	34	94	95	5311.38	1	37	80	81
5309.97	0	33	67	66	5311.41	0	34	93	92
5309.98	0	32	21	20	5311.50	1	36	55	56
5309.99	0	32	24	25	5311.55	0	32	28	27
5309.99	0	36	126	127	5311.55	1	38	99	100
5310.05	0	33	70	71	5311.56	0	32	31	32
5310.06	1	36	52	53	5311.61	0	34	96	97
5310.17	0	35	112	113	5311.76	1	37	78	77
5310.17	1	38	95	94	5311.80	0	33	71	70
5310.18	0	32	22	21	5311.80	1	36	53	52
5310.19	0	32	25	26	5311.81	0	32	29	28
5310.29	1	37	76	75	5311.82	0	32	32	33
5310.34	1	36	50	49	5311.83	0	36	125	124
5310.39	0	32	23	22	5311.86	0	35	111	110
5310.40	0	32	26	27	5311.88	Band head for υ"=2 to υ'=39 band			

TABLE IV--Continued

λ air (Å)	υ''	υ'	J''	J'	λ air (Å)	υ''	υ'	J''	J'
5311.89	0	33	73	74	5313.56	0	32	38	39
5311.98	1	38	97	96	5313.64	1	37	83	84
5312.00	1	36	56	57	5313.71	0	33	73	72
5312.08	0	32	30	29	5313.80	0	33	76	77
5312.09	0	32	33	34	5313.83	1	38	99	98
5312.13	1	37	81	82	5313.87	0	32	36	35
5312.19	0	35	114	115	5313.88	0	32	39	40
5312.25	0	34	94	93	5313.88	1	36	57	56
5312.31	1	36	54	53	5313.91	0	35	113	112
5312.32	0	36	128	129	5313.97	0	34	96	95
5312.36	0	32	31	30	5314.03	1	37	81	80
5312.37	0	32	34	35	5314.09	1	36	60	61
5312.43	0	33	71	70	5314.17	0	34	99	100
5312.45	0	34	97	98	5314.18	0	36	127	126
5312.46	1	38	100	101	5314.19	0	32	37	36
5312.51	1	36	57	58	5314.21	0	32	40	41
5312.51	1	37	79	78	5314.25	0	35	116	117
5312.52	0	33	74	75	5314.32	1	38	102	103
5312.64	0	32	32	31	5314.37	0	33	74	73
5312.65	0	32	35	36	5314.41	1	37	84	85
5312.82	1	36	55	54	5314.42	1	36	58	57
5312.88	0	35	112	111	5314.46	0	33	77	78
5312.88	1	37	82	83	5314.53	0	32	38	37
5312.90	1	38	98	97	5314.54	0	32	41	42
5312.93	0	32	33	32	5314.64	1	36	61	62
5312.95	0	32	36	37	5314.66	1	35	0	1
5313.00	0	36	126	125	5314.66	1	35	1	2
5313.03	1	36	58	59	5314.66	1	35	2	3
5313.07	0	33	72	71	5314.68	1	35	3	4
5313.11	0	34	95	94	5314.68	0	36	130	131
5313.16	0	33	75	76	5314.69	1	35	1	0
5313.22	0	35	115	116	5314.70	1	35	4	5
5313.24	0	32	34	33	5314.72	1	35	2	1
5313.25	0	32	37	38	5314.73	1	35	5	4
5313.27	1	37	80	79	5314.76	1	35	3	2
5313.31	0	34	98	99	5314.77	1	35	5	6
5313.34	1	36	56	55	5314.77	1	38	100	99
5313.39	1	38	101	102	5314.81	1	35	4	3
5313.49	0	36	129	130	5314.81	1	37	82	81
5313.55	0	32	35	34	5314.83	1	35	7	8
5313.55	1	36	59	60	5314.84	0	34	97	96

TABLE IV--Continued

λ air (Å)	υ''	υ'	J''	J'	λ air (Å)	υ''	υ'	J''	J'
5314.87	0	32	39	38	5315.80	0	33	79	80
5314.87	1	35	5	4	5315.82	1	35	17	18
5314.88	1	36	8	9	5315.87	0	36	131	132
5314.89	0	32	42	43	5315.93	0	34	101	102
5314.93	1	35	6	5	5315.93	1	35	15	14
5314.95	0	35	114	113	5315.96	0	32	42	41
5314.95	1	35	9	10	5315.97	0	32	45	46
5314.97	1	36	59	58	5315.97	1	35	18	19
5315.01	1	35	7	6	5315.98	1	37	86	87
5315.03	0	33	75	74	5316.00	0	35	115	114
5315.03	1	35	10	11	5316.08	1	35	16	15
5315.04	0	34	100	101	5316.10	1	36	61	60
5315.09	1	35	8	7	5316.13	1	35	19	20
5315.12	0	33	78	79	5316.22	1	38	104	105
5315.12	1	35	11	12	5316.25	1	35	17	16
5315.18	1	35	9	8	5316.30	1	35	20	21
5315.19	1	36	62	63	5316.33	1	36	64	65
5315.19	1	37	85	86	5316.34	0	32	43	42
5315.21	1	35	12	13	5316.35	0	32	46	47
5315.23	0	32	40	39	5316.35	0	35	118	119
5313.24	0	32	43	44	5316.38	0	33	77	76
5315.27	1	38	103	104	5316.39	1	37	84	83
5315.28	1	35	10	9	5316.42	1	35	18	17
5315.29	0	35	117	118	5316.48	0	33	80	81
5315.32	1	35	13	14	5316.48	1	35	21	22
5315.37	0	36	128	127	5316.57	0	36	129	128
5315.39	1	35	11	10	5316.60	1	35	19	18
5315.43	1	35	14	15	5316.61	0	34	99	98
5315.51	1	35	12	11	5316.66	1	35	22	23
5315.53	1	36	60	59	5316.68	1	36	62	61
5315.55	1	35	15	16	5316.68	1	38	102	101
5315.59	0	32	41	40	5316.72	0	32	44	43
5315.59	1	37	83	82	5316.74	0	32	47	48
5315.60	0	32	44	45	5316.78	1	37	87	88
5315.64	1	35	13	12	5316.79	1	35	20	19
5315.68	1	35	16	17	5316.82	0	34	102	103
5315.70	0	33	76	75	5316.85	1	35	23	24
5315.72	0	34	98	97	5316.91	1	36	65	66
5315.72	1	38	101	100	5316.99	1	35	21	20
5315.76	1	36	63	64	5317.06	0	35	116	115
5315.78	1	35	14	13	5317.06	1	35	24	25

TABLE IV--Continued

λ air (Å)	υ''	υ'	J''	J'	λ air (Å)	υ''	υ'	J''	J'
5317.07	0	33	78	77	5318.47	1	35	30	31
5317.08	0	36	132	133	5318.47	1	36	65	64
5317.12	0	32	45	44	5318.48	0	33	80	79
5317.14	0	32	48	49	5318.48	0	35	120	121
5317.17	0	33	81	82	5318.58	0	33	83	84
5317.19	1	37	85	84	5318.62	1	38	104	103
5317.19	1	38	105	106	5318.63	0	34	104	105
5317.20	1	35	22	21	5318.65	1	35	28	27
5317.27	1	35	25	26	5318.72	1	36	68	69
5317.27	1	36	63	62	5318.73	1	35	31	32
5317.41	0	35	119	120	5318.79	0	32	49	48
5317.42	1	35	23	22	5318.81	0	32	52	53
5317.49	1	35	26	27	5318.83	1	37	87	86
5317.50	1	36	66	67	5318.92	1	36	29	28
5317.51	0	34	100	99	5319.00	0	36	131	130
5317.52	0	32	46	45	5319.01	1	35	32	33
5317.54	0	32	49	50	5319.09	1	36	66	65
5317.59	1	37	88	89	5319.14	1	38	107	108
5317.65	1	35	24	23	5319.20	0	33	81	80
5317.65	1	38	103	102	5319.20	1	35	30	29
5317.72	0	34	103	104	5319.21	0	35	118	117
5317.72	1	35	27	28	5319.23	0	32	50	49
5317.77	0	33	79	78	5319.24	1	37	90	91
5317.78	0	36	130	129	5319.25	0	32	53	54
5317.86	1	36	64	63	5319.29	1	35	33	34
5317.87	0	33	82	83	5319.30	0	33	84	85
5317.89	1	35	25	24	5319.33	0	34	102	101
5317.94	0	32	47	46	5319.34	1	36	69	70
5317.96	0	32	50	51	5319.49	1	35	31	30
5317.96	1	35	28	29	5319.51	0	36	134	135
5318.01	1	37	86	85	5319.54	0	34	105	106
5318.10	1	36	67	68	5319.57	0	35	121	122
5318.13	0	35	117	116	5319.58	1	35	34	35
5318.13	1	35	26	25	5319.61	1	38	105	104
5318.16	1	38	106	107	5319.67	1	37	88	87
5318.21	1	35	28	30	5319.68	0	32	51	50
5318.29	0	36	133	134	5319.69	0	32	54	55
5318.36	0	32	48	47	5319.71	1	36	67	66
5318.38	0	32	51	52	5319.79	1	35	32	31
5318.39	1	35	27	26	5319.89	1	35	35	36
5318.41	0	34	101	100	5319.92	0	33	82	81
5318.41	1	37	89	90	5319.96	1	36	70	71

TABLE V

CALCULATED ABSORPTION LINE IN IODINE VAPOR,
6930Å TO 6950Å

λ_{air} (Å)	υ''	υ'	J''	J'	λ_{air} (Å)	υ''	υ'	J''	J'
6930.47	7	2	104	105	6932.63	8	3	16	17
6930.65	7	2	97	96	6932.64	8	3	9	8
6039.70	8	4	116	115	6932.73	8	3	17	18
6930.72	8	4	123	124	6932.75	8	3	10	9
6931.24	7	2	105	106	6932.81	7	2	107	108
6931.42	7	2	98	97	6932.84	8	3	18	19
6931.63	8	4	117	116	6932.86	8	3	11	10
6931.66	8	4	124	125	6932.96	8	3	19	20
6931.99	8	3	2	3	6932.98	8	3	12	11
6931.99	8	3	3	4	6932.99	7	2	100	99
6931.99	8	3	4	5	6933.08	8	3	20	21
6932.00	8	3	5	6	6933.10	8	3	13	12
6932.01	8	3	1	2	6933.22	8	3	21	22
6932.02	7	2	106	107	6933.24	8	3	14	13
6932.02	8	3	6	7	6933.36	8	3	22	23
6032.03	8	3	0	1	6933.38	8	3	15	14
6932.05	8	3	7	8	6933.51	8	3	23	24
6932.08	8	3	8	9	6933.53	8	3	16	15
6932.09	8	3	1	0	6933.54	8	4	119	118
6932.12	8	3	9	10	6933.56	8	4	126	127
6932.13	8	3	2	1	6933.60	7	2	108	109
6932.17	8	3	10	11	6933.66	8	3	24	25
6932.18	8	3	3	2	6933.69	8	3	17	16
6932.20	7	2	99	98	6933.78	7	2	101	100
6932.23	8	3	11	12	6933.83	8	3	25	26
6932.24	8	3	4	3	6933.85	8	3	18	17
6932.29	8	3	12	13	6934.00	8	3	26	27
6932.30	8	3	5	4	6934.02	8	3	19	18
6932.37	8	3	13	14	6934.18	8	3	27	28
6932.38	8	3	6	5	6934.20	8	3	20	19
6932.44	8	3	14	15	6934.36	8	3	28	29
6932.46	8	3	7	6	6934.39	8	3	21	20
6932.53	8	3	15	16	6934.40	7	2	109	110
6932.55	8	3	8	7	6934.50	8	4	120	119
6932.58	8	4	118	117	6934.53	8	4	127	128
6932.61	8	4	125	126	6934.56	8	3	29	30

TABLE V - Continued

λ_{air} (Å)	υ''	υ'	J''	J'	λ_{air}	υ''	υ'	J''	J'
6934.59	7	2	102	101	6937.83	8	3	35	34
6934.59	8	3	22	21	6937.88	7	2	106	105
6934.76	8	3	30	31	6938.08	8	3	43	44
6934.79	8	3	23	22	6938.13	8	3	36	35
6934.97	8	3	31	32	6938.39	8	3	44	45
6935.00	8	3	24	23	6938.43	8	4	124	123
6935.19	8	3	32	33	6938.44	8	3	37	36
6935.21	7	2	110	111	6938.46	8	4	131	132
6935.22	8	3	25	24	6938.53	7	2	114	115
6935.40	7	2	103	102	6938.71	8	3	45	46
6935.41	8	3	33	34	6938.72	7	2	107	106
6935.45	8	3	26	25	6938.76	8	3	38	37
6935.47	8	4	121	120	6939.03	8	3	46	47
6935.50	8	4	128	129	6939.08	8	3	39	38
6935.64	8	3	34	35	6939.36	8	3	47	48
6935.68	8	3	27	26	6939.38	7	2	115	116
6935.88	8	3	35	36	6939.42	8	3	40	39
6935.92	8	3	28	27	6939.43	8	4	125	124
6936.03	7	2	111	112	6939.46	8	4	132	133
6936.13	8	3	36	37	6939.57	7	2	108	107
6936.17	8	3	29	28	6939.70	8	3	48	49
6936.22	7	2	104	103	6939.76	8	3	41	40
6936.39	8	3	37	38	6940.05	8	3	49	50
6936.43	8	3	30	29	6040.11	8	3	42	41
6936.45	8	4	122	121	6940.23	7	2	116	117
6936.48	8	4	129	130	6940.41	8	3	50	51
6936.65	8	3	38	39	6940.43	7	2	109	108
6936.69	8	3	31	30	6940.45	8	4	126	125
6936.85	7	2	112	113	6940.46	8	3	43	42
6936.92	8	3	39	40	6940.48	8	4	133	134
6936.96	8	3	32	31	6940.77	8	3	51	52
6937.04	7	2	105	104	6940.83	8	3	44	43
6937.20	8	3	40	41	6941.10	7	2	117	118
6937.24	8	3	33	32	6941.14	8	3	52	53
6937.44	8	4	123	122	6941.20	8	3	45	44
6937.46	8	4	130	131	6941.29	7	2	110	109
6937.49	8	3	41	40	6941.47	8	4	127	126
6937.53	8	3	34	33	6941.49	8	4	134	135
6937.69	7	2	113	114	6941.52	8	3	53	54
6937.78	8	3	42	43	6941.58	8	3	46	45

TABLE V - Continued

λ_{air} (Å)	υ''	υ'	J''	J'	λ_{air} (Å)	υ''	υ'	J''	J'
6941.91	8	3	54	55	6945.73	8	3	63	64
6941.97	7	2	118	119	6945.74	7	2	115	114
6941.97	8	3	47	46	6945.80	8	3	56	55
6942.17	7	2	111	110	6946.19	8	3	64	65
6942.30	8	3	55	56	6946.26	8	3	57	56
6942.36	8	3	48	47	6946.45	7	2	123	124
6942.49	8	4	128	127	6946.65	7	2	116	115
6942.52	8	4	135	136	6946.66	8	3	65	66
6942.70	8	3	56	57	6946.68	8	4	132	131
6942.76	8	3	49	48	6946.72	8	4	139	140
6942.85	7	2	119	120	6946.74	8	3	58	57
6943.05	7	2	112	111	6947.14	8	3	66	67
6943.11	8	3	57	58	6947.22	8	3	59	58
6943.17	8	3	50	49	6947.36	7	2	124	125
6943.53	8	3	58	59	6947.57	7	2	117	116
6943.53	8	4	129	128	6947.63	8	3	67	68
6943.56	8	4	136	137	6947.70	8	3	60	59
6943.59	8	3	51	50	6947.75	8	4	133	132
6943.74	7	2	120	121	6947.78	8	4	140	141
6943.94	7	2	113	112	6948.12	8	3	68	69
6943.95	8	3	59	60	6948.20	8	3	61	60
6944.02	8	3	52	51	6948.29	7	2	125	126
6944.39	8	3	60	61	6948.50	7	2	118	117
6944.45	8	3	53	52	6948.63	8	3	69	70
6944.57	8	4	130	129	6948.70	8	3	62	61
6944.60	8	4	137	138	6948.83	8	4	134	133
6944.63	7	2	121	122	6948.86	8	4	141	142
6944.83	8	3	61	62	6949.14	8	3	70	71
6944.84	7	2	114	113	6949.21	8	3	63	62
6944.89	8	3	54	53	6949.23	7	2	126	127
6945.27	8	3	62	63	6949.44	7	2	119	118
6945.34	8	3	55	54	6949.65	8	3	71	72
6945.53	7	2	122	123	6949.73	8	3	64	63
6945.62	8	4	131	130	6949.91	8	4	135	134
6945.65	8	4	138	139	6949.95	8	4	142	143

TABLE VI

MEASURED ABSORPTION LINES IN IODINE VAPOR,
5300Å TO 5320Å

λ_{air} (Å)	λ_{air} (Å)	λ_{air} (Å)	λ_{air} (Å)
5300.03	5305.10	5309.76	5314.53
5300.13	5305.31	5309.86	5314.77
5300.19	5305.39	5309.93	5314.86
5300.29	5305.58	5310.05	5315.20
5300.48	5305.83	5310.11	5315.43
5300.55	5305.92	5310.30	5315.56
5300.62	5306.00	5310.46	5315.71
5301.00	5306.07	5310.51	5315.84
5301.05	5306.37	5310.63	5315.92
5301.21	5306.47	5310.71	5316.10
5301.33	5306.63	5310.77	5316.30
5301.43	5306.91	5310.94	5316.61
5301.51	5307.03	5311.07	5316.66
5301.72	5307.28	5311.15	5316.80
5301.88	5307.45	5311.38	5316.93
5301.93	5307.55	5311.56	5317.06
5302.27	5307.62	5311.64	5317.23
5302.34	5307.83	5311.81	5317.46
5302.44	5307.93	5311.88	5317.64
5302.66	5308.04	5311.96	5317.87
5302.81	5308.07	5312.13	5317.99
5302.89	5308.10	5312.30	5318.14
5303.19	5308.21	5312.41	5318.20
5303.30	5308.30	5312.68	5318.27
5303.40	5308.40	5312.82	5318.35
5303.77	5308.48	5312.96	5318.44
5303.87	5308.58	5313.08	5318.49
5303.95	5308.67	5313.26	5318.60
5304.15	5308.77	5313.46	5318.71
5304.29	5308.89	5313.57	5318.92
5304.37	5308.94	5313.68	5319.07
5304.49	5309.02	5313.88	5319.13
5304.62	5309.15	5314.11	5319.37
5304.71	5309.28	5314.20	5319.59
5304.79	5309.46	5314.29	5319.65
5304.88	5309.71	5314.41	5319.78
			5319.99

TABLE VII

MEASURED ABSORPTION LINES IN IODINE VAPOR, 6930Å TO 6950Å

λ_{air} (Å)	λ_{air} (Å)	λ_{air} (Å)
6930.25	6937.94	6943.23
6931.13	6938.28	6943.58
6932.01	6938.57	6944.03
6932.63	6938.89	6944.46
6933.40	6939.20	6944.91
6933.96	6939.53	6945.33
6934.93	6939.88	6945.79
6935.87	6940.18	6946.71
6936.22	6940.55	6947.15
6936.65	6940.90	6947.65
6936.89	6941.30	6948.12
6937.13	6941.67	6949.14
6937.42	6942.02	6949.67
6937.69	6942.86	

The second part of the iodine experiment involved spectroscopic studies of absorption of intense laser light near 5310Å. This radiation was obtained by frequency doubling of the Nd-glass laser output at 1.06μ. The experimental arrangement is described in Chapter VI of this paper. Figure 13 contains two typical exposures. The absorption spectrum of iodine is at the bottom of each exposure, the spectrum of the laser at the top of each exposure, and in the center of each exposure is the laser spectrum after it passed through the iodine.

The output light from the Nd-glass laser system is rated at 70 megawatts, but only 10 per cent is converted by frequency doubling to the 5310Å region. The 7 megawatts of converted light is distributed over 100 evenly spaced lines in a 20Å interval. Assuming an even distribution of energy, this gives 70 kilowatts in each line. Assuming also that complete absorption takes place on a line .05Å wide, the power absorbed is 35 kilowatts. At 50°C over 90 per cent of the energy of the laser beam was absorbed by the iodine. With focusing lenses, power densities up to 0.1 MC/cm^2 line were obtained. No indications of stimulated fluorescence, stimulated Raman or stimulated Rayleigh scattering were detected.

Uneven distribution of power over the laser output lines caused an occasional anomalous, very intense line. This line could not be controlled so as to place it directly in coincidence with an absorption line of iodine. Accidental coincidence was never observed.

Coincidence of the lines would have raised the power density at the iodine line by one to two orders of magnitude. It is of interest to note, however, that some of the laser lines are split by absorption lines of iodine.

The third part of the iodine experiment consisted of a measurement of absorption by ruby laser light at 6943Å. The results are shown in Figure 13. The spectrum of the laser output after it has passed through iodine is superimposed on the iodine absorption spectrum. No indications of interactions other than absorption were detected. Over 90 per cent of the laser energy was absorbed by the iodine vapor at 100°C. Power densities up to 100 MW/cm^2 were used.

B. Neodymium-Doped Glass

Stimulated emission of radiation at 1.06μ was obtained from neodymium-doped glass when it was optically pumped by ruby laser light that had been Raman shifted by passage through benzene. A typical output pulse is shown in Figure 14. The output pulse is less than 10 nanoseconds long. The rise time of the photomultiplier system prevented accurate measurements of pulses less than 10 nanoseconds long.

The stimulated emission was obtained with mirror L-3 (see Figure 11) in position "A" of the system shown in Figure 12. No mirror was used in position "B".

The system was near threshold when the ruby laser output

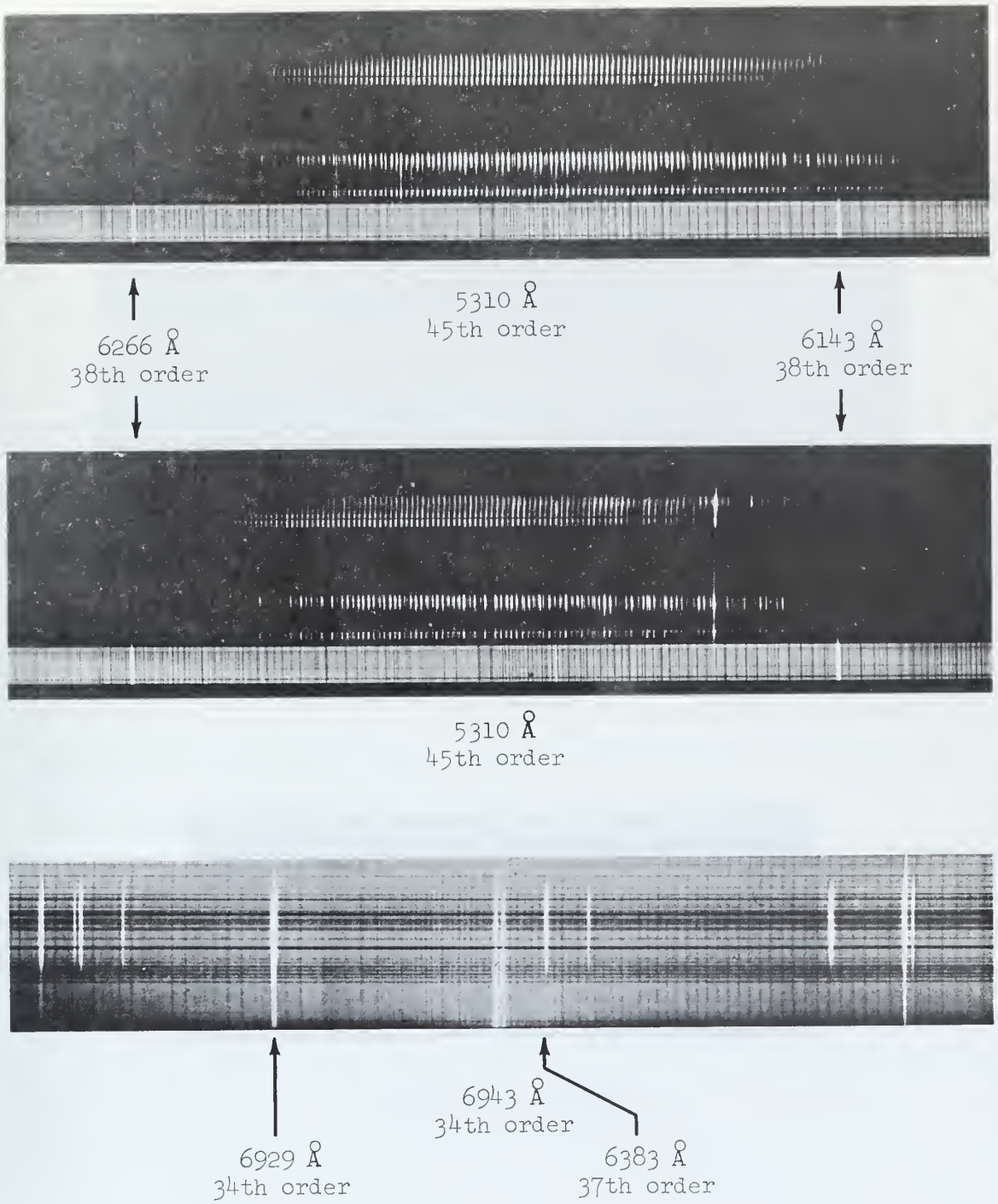

Figure 13. Spectra near 5310 Å and 6943 Å of Laser Absorption in Iodine Vapor.

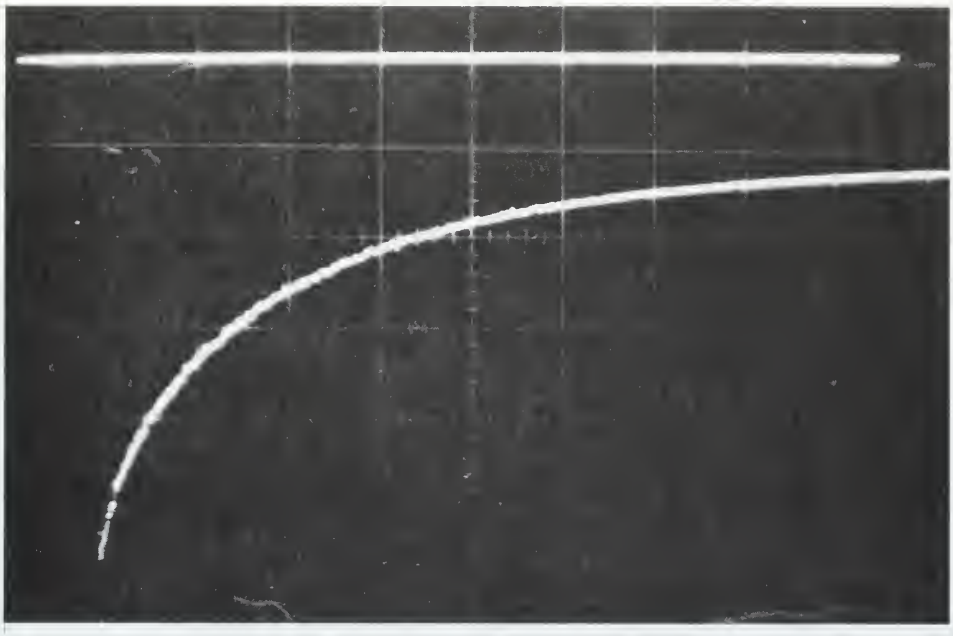

FLUORESCENCE
0.1 milliseconds/division

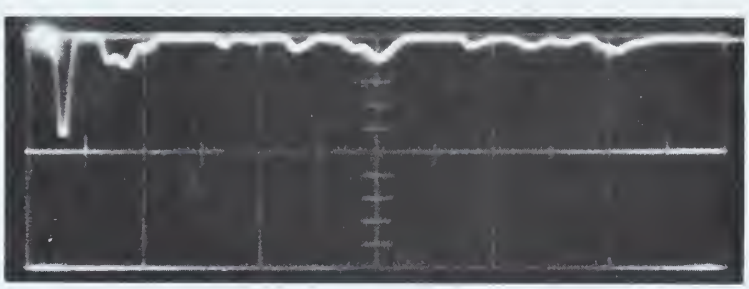

STIMULATED EMISSION
100 nanoseconds/division

Figure 14. Oscilloscope Traces of Fluorescence and of Stimulated Emission from Neodymium-Doped Glass at 1.06 microns.

was at 40 megawatts. Consistant operation, therefore, was not possible. At slightly lower power levels, however, it was possible to measure the fluorescence of the neodymium-doped glass at 1.06μ. Figure 14 contains an oscilloscope trace of this fluorescence. The fluorescence did not decay at an exact exponential rate. The half life of the fluorescence was initially 1×10^{-4} seconds, but it soon increased to 2×10^{-4} seconds. The discrepancy is probably due to the detection system rather than some unusual phenomenon.

It was not possible to record the stimulated emission using the low dispersion spectrograph and type I-Z plates due to the low sensitivity of the emulsion and the relatively low intensity of the radiation. The pulse power, as measured by the oscilloscope, was a factor of ten lower than that of the broad-band emission from benzene, which will be discussed next.

C. Benzene

Stimulated emission of light from benzene was observed in a broad spectral region from 9100Å to 10,900Å. Observations were made using the arrangement shown in Figure 12 with the exception that no focusing lens and no mirrors were in the system. When detection was made by spectrograph, the neodymium-doped glass rod was also removed and the light which passed through the optical

attenuator was focused on the slit of the spectrograph. No difference in the output was discernible when the $CoCl_2$ optical attenuator was replaced with a $CoBr_2$ optical attenuator. Figure 15 contains a spectrum of the observed emission as recorded on type I-Z plates using the low dispersion spectrograph. A mercury spectrum is superimposed as a reference.

The output consisted of a short pulse of 10 nanoseconds or less duration, as measured by the Tektronix 519 oscilloscope and the RCA 7102 photomultiplier. An example of the pulse trace from the Tektronix 519 is shown in Figure 16. The photomultiplier and monochromator were used to establish spectral limits of the emission because it was more sensitive than the type I-Z film for detection purposes.

The power in the stimulated emission was estimated by comparing the pulse height from radiation at 6943Å after it had passed through the system with the pulse height of the radiation at 1.04μ. Corrections were applied for the optical attenuators and spectral sensitivity of the photomultiplier. When the laser output was 40 megawatts, the stimulated pulse was estimated to be about 500 kilowatts peak power.

The threshold for this emission was measured to be about 25 ± 10 MW/cm^2. The threshold varied greatly, and it tended to increase after the laser was fired through the benzene several times.

The production of this broad-band stimulated emission has not

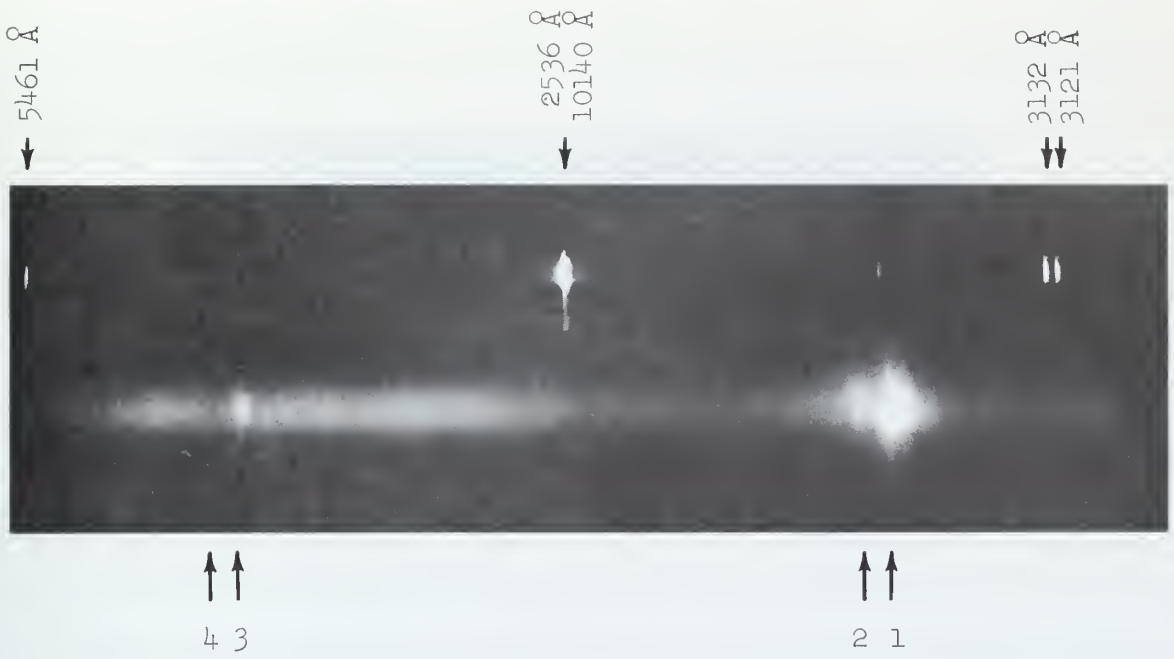

Figure 15. Spectrum of the Broad Band Stimulated Emission from Benzene. (1 refers to the 4th order Stokes shift of 991 cm^{-1}; 2 refers to the 1st order of the 991 cm^{-1} shift in combination with the 1st order 3064 cm^{-1} shift; 3 refers to the 5th order 991 cm^{-1} shift; and 4 refers to the 1st order 3064 cm^{-1} shift in combination with the 2nd order 991 cm^{-1} shift.)

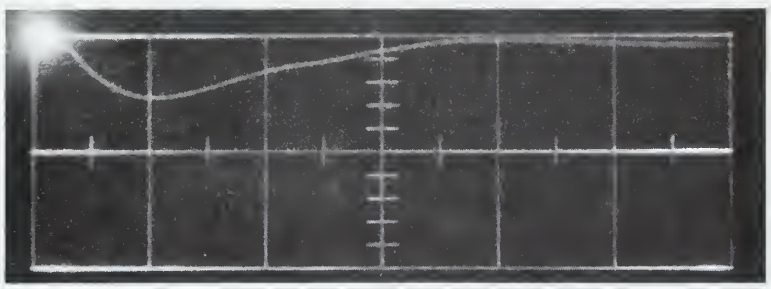

10 nanoseconds/division

Figure 16. Oscilloscope Trace of Stimulated Emission from Benzene at 1.03 microns.

previously been reported, and none of the present theories clearly explain its existence. Although the primary purpose of this paper is to report experimental results, some possible explanations of the broad-band emission are offered below.

Lallemand[40] reported broadening of the stimulated Raman lines to as much as 75Å in width. If this broadening were magnified by scattering in higher orders, and the correct combinations of higher order Stokes lines were used, it is conceivable that the result could appear to be a continuous spectrum.

Using the frequencies of the strong Raman lines given by Angus, Ingold, and Leckie,[41] the numbered arrows in Figure 15 were placed as follows: 1 is the fourth order shift for the 991 cm^{-1} line; 2 is the first order shift of the 991 cm^{-1} line in combination with the first order shift of the 3061 cm^{-1} line; 3 is the fifth order shift of the 991 cm^{-1} line; and 4 is the first order shift of the 3061 cm^{-1} line.

The numbered arrows 1, 2, and 3 clearly correspond to lines in the spectrum which stand out from the background of continuous emission. They appear to be separate from the background instead of the cause of the background.

Another possible explanation may be that the continuous scattering observed by Raman,[42] and commented on by Vankateswaram,[43] may be participating as a stimulated process. Regardless of whether these explanations are correct or not, the presence of this very broad band of stimulated emission is a new and interesting occurrence.

BIBLIOGRAPHY

1. T. H. Maiman, Nature 187, 493 (1960).

2. R. W. Hellwarth, Advances in Quantum Electronics (Columbia University Press, New York, 1961).

3. G. Eckhardt, R. W. Hellwarth, F. J. McClung, S. E. Schwarz, D. Weiner, and E. J. Woodbury, Phys. Rev. Lett. 9, 455 (1962).

4. R. Y. Chiao, C. H. Townes, and B. P. Stoicheff, Phys. Rev. Lett. 12, 592 (1964).

5. C. W. Cho, N. D. Foltz, D. H. Rank, and T. A. Wiggins, Phys. Rev. Lett. 18, 107 (1967).

6. G. A. Askar'yan, Soviet Phys. JETP 15, 1088 (1962).

7. R. Y. Chiao, E. Garmire, and C. H. Townes, Phys. Rev. Lett. 13, 479 (1964).

8. P. P. Sorokin and J. R. Lankard, IBM J. Res. Develop. 10, 162 (1966).

9. G. Briquet, J. M. Jego, and A. Terneaud, Appl. Phys. Lett. 14, 282 (1969).

10. P. M. Dirac, The Principles of Quantum Mechanics (Clarendon Press, Oxford, England, 1958), 4th ed.

11. D. Marcuse, Principles of Quantum Electronics (Unpublished manuscript, University of Utah, 1967).

12. L. Brillouin, Ann. Phys. (Paris) 17, 88 (1922).

13. T. A. Wiggins, R. V. Wick, and D. H. Rank, Appl. Opt. 5, 1069 (1966).

14. A. Yariv, Quantum Electronics (John Wiley and Sons, Inc., New York, 1967).

15. E. J. Woodbury and W. K. Ng, Proc. IRE 50, 2367 (1962).

16. R. W. Terhune, Bull. Am. Phys. Soc. 8, 359 (1963).

17. N. Bloembergen, Am. J. Phys. 35, 989 (1967).

18. P. Lallemand and N. Bloembergen, Phys. Rev. Lett. 15, 1010 (1965).

19. G. G. Bret and M. M. Denariez, Phys. Lett. 22, 583 (1966).

20. D. I. Mash, V. V. Morozov, V. S. Starnuov, and I. L. Fabelinskii, Soviet Phys. JETP Lett. 2, 25 (1965).

21. R. W. Wood, Phil. Mag. 21, 261 (1911).

22. R. W. Wood, Phil. Mag. 24, 673 (1912).

23. R. W. Wood, Phil. Mag. 26, 828 (1913).

24. G. Herzberg, Spectra of Diatomic Molecules (D. Van Nostrand Company, Princeton, New Jersey, 1950), 2nd ed.

25. M. Born and R. Oppenheimer, Ann. Physik 84, 457 (1927).

26. D. H. Rank and B. S. Rao, J. Mol. Spectr. 13, 34 (1964).

27. J. I. Steinfeld, R. N. Zare, L. Jones, M. Lesk, and W. Klemperer, J. Chem. Phys. 42, 25 (1965).

28. R. E. Honig, RCA Rev. 18, 195 (1957).

29. E. H. Carlson and G. H. Dieke, J. Chem. Phys. 29, 229 (1958).

30. L. F. Johnson, J. Appl. Phys. 34, 897 (1963).

31. G. H. Dieke and H. M. Crosswhite, Appl. Opt. 2, 675 (1963).

32. L. F. Johnson, Quantum Electronics III (Columbia Press, New York, 1964), p 1021.

33. Owens-Illinois, Inc., Advertisement Brochure for ED-2 Glass, (Owens-Illinois, Inc., Toledo, Ohio, 1967).

34. D. Röss and G. Zeidler, Z. Naturforsh. 21a, 336 (1966).

35. Radio Corporation of America, Phototubes and Photocells, Technical Manual PT-60, (Lancaster, Pennsylvania, 1963).

36. P. P. Sorokin, N. S. Shiren, J. R. Lankard, E. C. Hammond, and T. G. Kazyaka, Appl. Phys. Lett. 10, 44 (1967).

37. W. Brode, Chemical Spectroscopy (John Wiley and Sons, Inc., New York, 1943).

38. Eastman Kodak Company, Kodak Photographic Plates (Eastman Kodak Company, Rochester, New York, 1953).

39. Polaroid, "How to Use Polaroid Type 413 Land Infrared Film", (Instruction sheet from film package, 1969).

40. P. Lallemand, Appl. Phys. Lett. 8, 276 (1966).

41. W. R. Angus, C. K. Ingold, and A. H. Leckie, J. Chem. Soc. 925 (1936).

42. C. V. Raman, Nature 121, 619 (1928).

43. S. Venkateswaran, Nature 122, 506 (1928).

VITA

Lorin W Brown was born in Cedar City, Utah, on July 19, 1937. He is the seventh of ten children born to Mr. and Mrs. John M. Brown of Cedar City. His elementary and secondary education was obtained in the public school system. He graduated from Cedar High School in May, 1955. He attended the College of Southern Utah at Cedar City, Utah, and was awarded an Associate of Science degree in May, 1957.

In September, 1957, Mr. Brown received an appointment as a regular midshipman in the Naval Reserve Officer Training Corps and enrolled at the University of Utah. He was graduated with honors and received his Bachelor of Science degree in June, 1959.

From September, 1959, until July, 1961, he attended the University of Utah while working toward a doctorate in Physics. In July, 1961, he was commissioned as an Ensign in the United States Navy and called to active duty. He received training as a Naval Aviator and was assigned to Attack Squadron Ninety-Four. The Distinguished Flying Cross and fourteen Air Medals were awarded to him for his participation in this nation's operations in Vietnam.

Mr. Brown returned to the University of Utah in September, 1966, as an Assistant Professor of Naval Science. In September, 1967, the Bureau of Naval Personnel assigned Mr. Brown to full time duties as a graduate student.

He is a member of Sigma Pi Sigma, Pi Mu Epsilon, the American Physical Society, and the Optical Society of America.

Mr. Brown is married to Marilynn Thompson of River Heights, Utah, and they have a son, Christopher, who is six months old.

Thesis 115639
B818 Brown
Interactions of intense coherent light with iodine vapor, neodymium-doped glass, and benzene.